NASA TECHNICAL NOTE

NASA TN D-4411

NASA TN D-4411

ANALYTICAL COMPARISON OF RANKINE CYCLE SPACE RADIATORS CONSTRUCTED OF CENTRAL, DOUBLE, AND BLOCK-VAPOR-CHAMBER FIN-TUBE GEOMETRIES

by Henry C. Haller and Seymour Lieblein

Lewis Research Center
Cleveland, Ohio

NATIONAL AERONAUTICS AND SPACE ADMINISTRATION • WASHINGTON, D. C. • FEBRUARY 1968

ANALYTICAL COMPARISON OF RANKINE CYCLE SPACE RADIATORS CONSTRUCTED OF CENTRAL, DOUBLE, AND BLOCK-VAPOR-CHAMBER FIN-TUBE GEOMETRIES

By Henry C. Haller and Seymour Lieblein

Lewis Research Center
Cleveland, Ohio

NATIONAL AERONAUTICS AND SPACE ADMINISTRATION

For sale by the Clearinghouse for Federal Scientific and Technical Information
Springfield, Virginia 22151 – CFSTI price $3.00

ANALYTICAL COMPARISON OF RANKINE CYCLE SPACE RADIATORS CONSTRUCTED OF CENTRAL, DOUBLE, AND BLOCK-VAPOR-CHAMBER FIN-TUBE GEOMETRIES

by Henry C. Haller and Seymour Lieblein

SUMMARY

An analytical comparison of flat direct-condensing radiators constructed of three different finned tube geometries was made over a wide range of design variables for a 500-day mission, 500-kilowatt output high-temperature Rankine space electric power generating system which used potassium as the cycle working fluid. The fin-tube configurations considered were the central, the double, and the block vapor-chamber geometries. The solid conducting fin geometries (central and double fin) were composed of stainless-steel-clad copper fins. The vapor-chamber fin radiator was evaluated for both stainless-steel-clad and all stainless-steel fins.

The vapor-chamber fin-tube radiator consistently showed a significantly lower weight per kilowatt output (specific weight) than the two solid conducting fin radiators. The relative weight advantage of the vapor-chamber fin-tube radiator was decreased somewhat when the comparison was based on specified heat rejection at the end of the mission. It was also shown that the magnitude of the radiator specific weight varied substantially as the radiator heat-rejection rate was varied due to different prescribed values of cycle component efficiencies.

A relatively small reduction in planform area per kilowatt output (specific planform area) at the least weight condition was indicated for the vapor-chamber fin-tube radiator compared with the solid conducting fin-tube configurations. However, this difference in specific planform area could easily be minimized by designing the solid conducting fin radiators for off-least-weight conditions with only a very small increase in specific weight.

In general, the vapor-chamber fin-tube radiator can utilize larger tube diameters and fewer number of tubes than the solid conducting geometries with the least increase in specific weight and planform area. Furthermore, except for a relatively small effect on the planform area required for specified final heat rejection and the specific weight at prescribed initial heat rejection, the choice of vapor-chamber fin material had negligible effect on the weight and geometric characteristics of the vapor-chamber fin radiator.

INTRODUCTION

Several studies on waste-heat radiators for Rankine cycle space-power generating systems (e.g., refs. 1 to 5) have considered fin-tube arrangements employing solid conducting fins between fluid carrying tubes. Solid conducting fin-tube arrangements investigated in these studies consisted of central fin (refs. 1 to 3), double fin. and open fin-tube radiators (refs. 4 and 5).

In order to increase the radiating effectiveness of the solid fin radiator and thereby decrease weight and planform area, the vapor-chamber fin-tube concept was analyzed for high- and low-power-level Rankine systems in references 6 and 7, respectively. The vapor-chamber fin concept proposes to reduce radiator weight and area by providing for an essentially isothermal fin between tubes. In one approach, this can be accomplished by using a double-wall fin between tubes to form a hollow chamber which contains a fluid-soaked capillary medium along the inner surfaces.

Preliminary comparative analysis of an all-columbium radiator for a 500-kilowatt Rankine cycle electric power output system and of a beryllium fin and armor radiator for a 1-megawatt system were presented in reference 6. These studies, which were based on the tube armor block configuration with a single value of tube nonpuncture probability of 0.995, indicated that the vapor-chamber fin-tube radiator concept can result in a sizable weight advantage, substantially smaller planform area, fewer number of tubes, and larger tube diameters than the central and double fin-tube radiators. Results of an analysis of the vapor chamber fin radiator for a low-power-level, low-temperature-level system (ref. 7) indicated the vapor fin radiator had a lower weight than the solid conducting geometires for values of nonpuncture probability greater than 0.95. The vapor-chamber fin geometry always gave a substantially smaller planform area.

However, structural complexities and disadvantages in the use of vapor-chamber fin geometries were also revealed. In order to maintain a reasonable survival probability for the vapor-chamber fin without using large fin thicknesses, it was necessary to compartmentalize the vapor-chamber fins into many individual segments by the use of transverse and longitudinal bulkheads. Radiator weight can be minimized by the use of a large number of fin segments, which might involve problems in the sealing of the individual segments. On the other hand, if a relatively small number of fin segments are used, the fin segment planform area might be large, so that stress and deflection problems might arise within the box-like structure of the vapor-chamber segments. Thus, it is desirable to obtain a more realistic evaluation of the theoretical weight and area gains achievable with the use of the vapor-chamber fin concept. In this way its potential applicability to space radiator design may be properly assessed.

This investigation is a further analytical comparison of the weight and geometry characteristics of space radiators with block vapor-chamber fin-tube, central fin-tube,

and double fin-tube geometries over a wider range of variables than considered previously (ref. 6). Numerical calculations using an electronic digital computer, are conducted for a planer direct-condensing radiator employing design inputs characteristic of a 500-kilowatt Rankine electric power generating cycle using potassium as the working fluid. Stainless-steel armor, and both stainless-steel and stainless-steel-clad copper fins are considered as the radiator materials of construction.

Radiator weight and geometry characteristics are determined for a range of variables such as tube inside diameter, fin profile ratio, and tube and header meteroid nonpuncture probability. For the vapor-chamber fin-tube geometry, the fin segment planform area, the percent of surviving fin segments, and the effects of radiator fin material were also investigated. Comparisons are made at identical design conditions with recently revised meteroid hazard inputs and material constants for the meteroid impact relations. Also investigated was an estimation of radiator weight and area characteristics for the case of fixed design heat-rejection capability at the end of the mission, and also for variations in cycle design inputs.

ANALYSIS

The relative comparisons of the three radiator geometries used cycle relations and design assumptions previously developed in references 2, 5, and 6, with the exception of revised meteroid protection criteria. These criteria included a revised particle density and velocity along with new experimental values of material factors for perforation or spall due to hypervelocity impact. Variations in cycle component efficiencies were also considered.

Radiator Configurations

The general radiator panel configuration considered for the analysis is shown in figure 1. The configuration illustrated is a flat-plate condensing radiator radiating hemispherically to space from both sides. Vapor from the turbine is distributed to the finned tubes by the central vapor header. The heat radiated from the vapor header and finned tubes causes the vapor to condense. The condensate is then subcooled and collected in the outer liquid headers before being returned to the condensate pump.

The detailed cross-sectional drawings of the three geometries to be compared are shown in figure 2. The central fin-tube geometry of figure 2(a) consists of a rectangular fin attached to two round tubes. The detailed cross-section drawing of the double fin-tube composed of tube armor block and two rectangular fins is shown in figure 2(b). This

geometry has a practical application in its ability to act as a bumper screen that will afford protection against meteroid impact damage on the tube block side walls. The vapor chamber fin-tube geometry of figure 2(c) consists of a tube armor block to provide meteoroid protection and two rectangular fins forming a sealed enclosed chamber between adjacent tubes. A capillary flow medium such as narrow grooves, woven wire mesh, or fibrous matt lines the inner surfaces of the fin chamber and is saturated with a heat-transport fluid. The fluid used should provide a saturation pressure at the chamber operating temperature that is structurally compatible with the chamber construction.

Inasmuch as the vapor chamber will lose its heat-transport action if a puncture and loss of transport fluid occurs, the long fin chambers are divided into sealed segments or compartments by numerous transverse bulkheads (fig. 3). The actual dimensions of the fin resulted from an optimization procedure which included meteroid protection considerations for the fin. The calculation procedure of reference 8 was used for the meteoroid puncture criterion for the fins with vulnerable area taken as the exposed surface of the fin segment.

The vapor header for all configurations is assumed to be a hollow paraboloid whose wall thickness is equal to the meteoroid protection armor thickness required by the tubes δ_a. (All symbols are defined in appendix A.) The parabolic shape is intended to produce a constant velocity in the header. For simplicity, the liquid header was designed with a constant diameter at a prescribed outlet fluid velocity. The liquid header also has a wall thickness equal to the meteoroid armor thickness obtained for the tubes. No heat radiation or subcooling was credited to the liquid header.

Material Considerations

The radiator materials considered are the readily available or conventional metals, namely, stainless steel or stainless-steel-clad copper. Stainless steel was prescribed as the tube and armor material, and stainless-steel-clad copper was used as the fin material for all three fin-tube geometries. Stainless-steel-clad copper fins were used for the solid-conducting central and double fin-tube geometries because the high thermal conductivity of the copper would reduce planform area, fin thickness, and thus, radiator weight. The composite material with the stainless-steel cladding is necessary because of the poor strength and high sublimation rate of copper at temperatures above 1460° R (811° K). All stainless-steel fins were not considered for the solid conducting fin geometries because the low thermal conductivity of stainless steel produces comparatively heavy radiators.

The stainless-steel-clad copper fin material is advantageous for vapor-chamber fin radiators because its high thermal conductivity is beneficial in the event of segment puncture. When a vapor fin segment is punctured, the capillary fluid is lost and the fin will

then operate as a solid conducting fin element. It is, therefore, desirable to maintain the heat conducting ability of the fin as high as possible in order to reduce the thermal degradation of the radiator. Stainless steel was investigated as a fin material for the vapor-chamber fin-tube radiator because it is a good structural material as well as a good meteoroid bumper material.

In order to use the composite material fins in the existing radiator design program, it was necessary to treat them as single-material fins with effective values of physical properties such as thermal conductivity, density, and modulus of elasticity. A two-dimensional thermal analysis was carried out in reference 9 to determine an effective thermal conductivity for stainless-steel-clad copper. The results of the investigation of reference 9 indicated that the exact formulation of effective conductivity of such a radiating fin is very nearly equal to the effective conductivity of the clad fin with conduction along the length of the fin only. As a consequence, the clad fins were treated in existing radiator design programs by considering the clad fin to be a fin of a single material with thermal conductivity equal to the simplified effective conductivity based on only the material thickness ratio t_{ss}/t_{cu} (fig. 4) and on the conductivities of the two materials k_{cu} and k_{ss}. The resultant expression for effective conductivity is

$$k_{eff} = \frac{\left(\frac{t_{ss}}{t_{cu}}\right)k_{ss} + k_{cu}}{1 + \left(\frac{t_{ss}}{t_{cu}}\right)} \tag{1}$$

The effective density for weight calculations was obtained as

$$\rho_{eff} = \frac{\left(\frac{t_{ss}}{t_{cu}}\right)\rho_{ss} + \rho_{cu}}{1 + \left(\frac{t_{ss}}{t_{cu}}\right)} \tag{2}$$

The effective modulus of elasticity used in the relations for determining metoeroid impact damage was obtained in a manner similar to equation (1) because no information is available for the exact treatment of this physical property. This equation is

$$E_{eff} = \frac{\left(\frac{t_{ss}}{t_{cu}}\right)E_{ss} + E_{cu}}{1 + \left(\frac{t_{ss}}{t_{cu}}\right)} \tag{3}$$

Material physical properties used in the calculations are listed in table I.

TABLE I. - MATERIAL PHYSICAL PROPERTIES AT 1700° R (945° K)

Material	Density, ρ		Thermal conductivity, k		Modulus of elasticity, E	
	lb/ft^3	kg/m^3	Btu/(hr)(ft)(°F)	W/m-°K	lb/ft^2	N/m^2
Stainless steel	500	8010	13.7	23.7	0.310×10^{10}	14.83×10^{10}
Copper	530	8490	198	342	$.0576\times10^{10}$	2.76×10^{10}

Meteroid Impact Damage Relations

For the vapor-chamber fin-tube geometry and the double fin-tube geometry of figure 2, the tube can be damaged by impacting meteoroids in two general ways. (1) The first is by any primary impacts occurring on the outer exposed surfaces of the tube block. These impacts are assumed to obey the conventional armor penetration and damage relations developed for tubes with vulnerable area given by $4\,R_b Z N_T$. (2) A second damage source can arise from a spray of particles on the armor block side surface, $4(R_o - t)ZN_T$, resulting from impacts on the fin surfaces. However, in view of the bumper action involved and the obliquity of the secondary impacts, a reduction will be allowed in the armor thickness required by the tube block sidewall to resist the effects of these secondary impacts. Parametric relations were unavailable for the precise determination of this sidewall thickness as a function of the radiator design variables involved, so that for ease of calculation the tube block sidewall thickness was included in the program as a ratio of the tube block armor protection thickness (δ_s/δ_a). The tube armor thickness for the central fin-tube geometry is determined by assuming that primary impacts occur on the peripheral area of the tube. This area, which is considered as the vulnerable area, is given by $\pi D_o Z N_T$.

The tube wall armor thickness and vapor-chamber fin outer-wall thickness relations were based on the following general expression:

$$\delta = \gamma a \left(\frac{6}{\pi \rho_p}\right)^{1/3} \left(\frac{\rho_p}{\rho_a}\right)^{1/2} \left(\frac{V_p}{\sqrt{\frac{E_a g}{\rho_a}}}\right)^{2/3} \left(\frac{\alpha A_v \tau}{-\ell n\, P(O)}\right)^{1/3\beta} \left(\frac{1}{\beta + 1}\right)^{1/3\beta} \tag{4}$$

The resultant equation for the tube armor thickness δ_a is

$$\delta_a = \frac{C \gamma a_t \left[\frac{A_v \tau}{-\ell n\, P(O)_t}\right]^{0.249}}{E_a{}^{1/3} \rho_a{}^{1/6}} \tag{5}$$

and for the vapor-chamber fin thickness

$$t = \frac{C \gamma a_f \left[\frac{2A_{seg} \tau}{-\ell n\, P(O)_f}\right]^{0.249}}{E_{eff}{}^{1/3} \rho_{eff}{}^{1/6}} \tag{6}$$

The equations for tube wall armor thickness and vapor-chamber fin thickness were determined using the recently available meteoroid data which determined the value of the constant C:

Particle velocity, V_p, ft/sec; m/sec	65 000; 19 800
Particle density, ρ_p, lb/ft^3; g/cm^3	12.5; 0.20
Penetration formula constant, α, $lb^\beta/(ft^2)(day)$; $g^\beta/(m^2)(day)$	0.147×10^{-13}; 0.571×10^{-9}
Penetration formula constant, β	1.34
Constant C, U.S. customary units; SI units	3.36; 88.8

In both equations, δ_a and t are in inches (or cm).

For the vapor-chamber fin, the planform area of each segment, $A_{seg} = 2\ell \times b$ was designated an independent variable. The individual segment area and the radiator planform area then determined the total number of fin segments N. The fin thickness t was based on a given probability S that a certain percentage of the segments N_s/N would remain unpunctured at the end of the design lifetime of the radiator. The individual fin segment nonpuncture probability $P(O)_f$ is a function of S and N_s/N (ref. 6).

The term γ in equations (5) and (6) is the impact cratering coefficient of the material. The terms a_t and a_f in the equations are damage thickness factors which depend on the armor material and the type of meteoroid damage allowable (i.e., perforation, spall, or dimple). For the tubes, a_t was taken as the value at incipient spall. This value is adequate to prevent perforation, but not great enough to guarantee that there will not be spalling off the tube inner surface. For the segmented vapor-chamber fins, the damage thickness factor a_f was taken as the value at perforation, that is, the value corresponding to a fin thickness just equal to the thickness that will be penetrated by the meteoroids.

The materials cratering coefficient γ and the damage factors for the tubes and fins a_t and a_f are shown for the two radiator materials in table II. The information contained therein was obtained from reference 10 and from preliminary unpublished experimental data.

TABLE II. - IMPACT FACTORS AT 1700° R (945° K)

Material	Cratering coefficient	Damage thickness factors	
		Fin perforation, a_f	Tube spall, a_t
Stainless steel	1.9	1.4	1.85
Stainless-steel-clad copper	2.1	.8	----

Program Inputs

Calculation program inputs required were cycle parameters, properties of the materials of construction and the cycle fluid, meteoroid protection criterion, fin-tube geometric parameters (e.g., tube internal diameter and fin profile ratio), and vapor-chamber fin heat-transfer parameters.

Design conditions for the radiators were assumed to be representative of a 500-kilowatt potassium Rankine cycle. Pertinent program inputs required for the three radiator fin-tube geometries to be analyzed are those given previously in tables I and II plus additional inputs as given in table III. These are used throughout, unless otherwise specified.

In view of the numerous variables and unknowns associated with the thermal and physical properties of stainless-steel-clad copper at design temperatures, an initial investigation was made to determine the sensitivity of minimum radiator weight and fin geometry to these variables and to select representative values for the comparison cal-

TABLE III. - CALCULATION PROGRAM INPUTS

Maximum cycle temperature, T_M, ^oR; ^oK	2460; 1365
Radiator fluid inlet temperature, T_R, ^oR; ^oK	1700; 945
Degrees of subcooling, ^oR; ^oK	100; 55.5
Turbine efficiency, η_t	0.75
Generator efficiency, η_g	0.90
Power availability factor, K_p	0.90
Electrical power output, Pe, kW	500
Radiator surface emittance	0.90
Space sink temperature, ^oR; ^oK	0; 0
Vapor-chamber boiling heat-transfer coefficient, Btu/(hr)(ft^2)(^{o}F); W/(m^2)(^{o}K)	10^4; 5.67×10^4
Vapor-chamber condensing heat-transfer coefficient, Btu/(hr)(ft^2)(^{o}F); W/(m^2)(^{o}K)	10^4; 5.67×10^4
Vapor-chamber capillary weight, lb/ft^2; kg/m^2	0.2; 0.976
Vapor-chamber transverse bulkhead thickness, in.; cm	0.025; 0.0635
Tube and header nonpuncture probability, $P(O)_t$	0.90 to 0.995
Overall fin nonpenetration probability, S	0.90
Ratio of surviving to design fin segments, N_s/N	0.75
Tube block sidewall thickness ratio, δ_s/δ_a	0.25
Mission time, day	500
Tube inside diameter, D_i, in.; cm	1/4 to 1; 0.635 to 2.54
Vapor chamber fin profile ratio, l/R_b	4 to 8
Solid conducting fin profile ratio, L/R_o	1 to 8
Conductance parameter, N_c	0.1 to 1.5
Stainless-steel clad to copper thickness ratio, t_{ss}/t_{cu}	0.40
Vapor-chamber fin segment planform area, A_{seg}, in.^{2}; cm^2	30; 193.5
Vapor header pressure drop ratio[a], $\Delta P/P$	0.02
Radiator-tube pressure drop ratio[a], $\Delta P/P$	0.05
Liquid header exit velocity (constant diameter), ft/sec; m/sec	4; 1.22
Cycle fluid liquid viscosity, lb/(ft)(sec); N-sec/m^2	0.931×10^{-4}; 1.384×10^{-4}
Cycle fluid liquid specific heat, Btu/(lb)(^{o}F); J/(kg)(^{o}K)	0.1842; 771.0
Cycle fluid liquid density, lb/ft^3; kg/m^3	42.57; 682.0
Cycle fluid vapor viscosity, lb/(ft)(sec); N-sec/m^2	0.597×10^{-5}; 0.889×10^{-5}
Cycle fluid vapor specific heat, Btu/(lb)(^{o}F); J/(kg)(^{o}K)	0.1268; 530

[a]Where P refers to the pressure at the vapor header inlet and the tube inlet, respectively.

culations. These results are presented in appendix B. A similar discussion of the selection of the representative values of the input variables for determining the geometry, weight, and heat-transfer characteristics of the vapor-chamber fin-tube radiator is given in appendix C.

Calculation Procedure

Calculations were performed using an iterative procedure programmed into an electronic digital computer. The calculations were based on the relations and procedures described in references 2, 5, and 6 in conjunction with the inputs presented previously. The weights obtained from the radiator optimization calculation were initially plotted as a function of the profile ratio l/R_b for the vapor-chamber fin and the profile ratio L/R_o for the solid conducting fin geometries to obtain the minimum value of specific weight W/Pe for each choice of tube inside diameter. Sample results for the vapor-chamber fin-tube geometry showing the variation in specific weight as a function of l/R_b are plotted for representative conditions in figure 5. A minimum weight point is established at a specific value of l/R_b. Similar results are shown for the solid-conducting double and central fin-tube geometries in figure 6. Values of the fin conductance parameter N_c are also shown on the figures. The results shown in figure 6 were obtained by initially optimizing W/Pe as a function of fin profile ratio L/R_o for each choice of N_c.

The minimum values of W/Pe for a given tube inside diameter, as obtained from the curves such as those in figures 5 and 6, were then plotted as a function of tube inside diameter for a range of diameters from 1/4 to 1 inch (0.63 to 2.54 cm) in order to establish the least-weight configuration for all diameters.

COMPARISON OF RESULTS

The three fin-tube configurations (the vapor-chamber fin-tube, the solid conducting central, and double fin-tube radiators) are compared in this section on the basis of weight and geometry for representative design variables.

Radiator Weight

Specified initial heat rejection. - The calculation procedure presents results for configurations required to reject the design waste-heat load at the start of the powerplant lifetime. A comparison of the minimum specific weight results for this case obtained

from figures 5 and 6 along with results for additional tube inside diameters, are shown in figure 7 for the three fin-tube geometries for $P(O)_t = 0.98$ and representative design inputs. It is observed from the figure that the vapor-chamber fin-tube radiator yields the least specific weight over the entire range of tube diameters investigated. The least specific weights were 2.90 pounds per kilowatt (1.28 kg/kW) at 0.53-inch (1.35-cm) diameter for the vapor-chamber fin-tube radiator with clad fins, 3.86 pounds per kilowatt (1.75 kg/kW) at 0.31-inch (0.79-cm) diameter for the double fin-tube radiator, and 4.75 pounds per kilowatt (2.15 kg/kW) at 0.47-inch (1.20-cm) diameter for the central fin-tube radiator. Thus, for the least-weight condition, the vapor-chamber fin-tube radiator with $\delta_s/\delta_a = 0.25$ yields a 40-percent weight reduction over the central fin-tube geometry and a 25-percent reduction over the double fin-tube geometry.

The tube, header, and fin percent weight breakdown for the three fin-tube geometries at the least-weight condition for $P(O)_t = 0.98$ and $t_{ss}/t_{cu} = 0.40$ is given in the following table.

TABLE IV. - RADIATOR WEIGHT BREAKDOWN

Configuration	Percent of total weight		
	Headers	Tubes	Fins
Central fin-tube	20.0	63.3	16.7
Double fin-tube[a]	23.9	58.1	18.0
Vapor-chamber fin-tube[a]	18.2	52.7	29.1

[a] $\delta_s/\delta_a = 0.25$.

There would be little difference in the weight of the vapor-chamber fin-tube radiator if stainless steel instead of stainless-steel-clad copper were used for the fin material. Most of the weight in this configuration is in the stainless-steel armor block and headers (e.g., around 71 percent for $P(O)_t = 0.98$) and the densities of the composite material and the stainless steel are about equal. It is also noted in figure 7 that, as diameter is increased past the value at least weight, the specific weight of the double fin-tube radiator increases very rapidly, while both the vapor-chamber fin-tube and central fin-tube radiators increase only moderately with a nearly constant percentage difference between the two configurations.

The effect of varying the tube nonpuncture probability $P(O)_t$ on radiator least specific weight for the three fin-tube geometries is shown in figure 8. There is a gradual increase in weight for all three geometries as the nonpuncture probability increases from 0.90 to 0.995. The vapor-chamber fin-tube radiators yield lower specific weights (for both fin materials) than the solid conducting central and double fin-tube geometries. In general, the vapor-chamber radiators yield a specific weight 13 to 29 percent lower than

the double fin-tube geometry, and from 28 to 45 percent lower than the central fin-tube geometry for the design inputs used.

The curves for the vapor-chamber fin cases of figures 7 and 8 were calculated for the case of the same initial power; that is, the effect of fin punctures on radiator heat-rejection capability was neglected. When a vapor-chamber fin segment is punctured, it will lose its capillary fluid and hence will no longer operate as a vapor-chamber fin. However, the fins of the chamber will receive heat by conduction from adjacent tubes and fins and by radiation from the adjacent tube and bulkhead surfaces. Thus, a radiation capability comparable to a solid conducting fin will be maintained. Solution of the actual physical case of a punctured segment requires a detailed two-dimensional study of the fin chamber heat transfer. However, for simplicity, calculations of degraded radiation for the vapor-chamber radiators were restricted to one-dimensional heat transfer along the fins for the case of isolated chamber puncture (adjacent segments operative). Analyses for the more complex case of adjacent segment punctures are given in references 6 and 7.

Figure 9 shows the calculated variation of ratio of final to initial heat rejection of the radiator as a function of percent of surviving segments at the end of the mission. The high thermal conductivity stainless-steel-clad copper fin material results in less degradation in heat-rejection potential. The decrease in the heat-rejection ratio with decreasing surviving segments is brought about by a decrease in fin thickness accompanying the decrease in survival percentage as well as by the decrease in nonpunctured area.

Specified final heat rejection. - In some instances it may be desirable to maintain the design heat-rejection potential throughout the lifetime of the powerplant. In this case, because thermal degradation is involved in the operation of vapor-chamber fins, the vapor-chamber fin radiators should be designed for the required heat rejection at the end of the mission. If constant radiator inlet temperature is also specified, this would require an overdesign of the vapor-chamber fin-tube radiators, that is, an increase in area above that required for the nonpuncture case presented in figure 8. Thus, an increase in radiator specific weight will be incurred relative to the solid-conducting fin radiators which undergo no comparable thermal degradation.

An indication of the maximum increase in vapor-chamber radiator weight when designed for specified final heat-rejection capability can be obtained, if it is assumed, for simplicity, that the percentage increase in required area is equal to the percentage decrease in final heat rejection as given in figure 9 and that the percentage increase in radiator weight is equal to the percentage increase in area. A comparison of radiator least specific weight for the two cases of specified initial heat rejection and specified final heat rejection on this basis is shown in figure 10(a) for the all-stainless steel and stainless-steel-clad copper fin radiator for $P(O)_t = 0.98$. Also included in the figure are the two solid conducting fin radiators.

For the vapor-chamber fin design cases at specified final heat rejection and tempera-

ture, a least-specific weight is obtained for values of N_s/N of 0.65 to 0.75. The stainless-steel-clad copper fin radiator at this condition is superior to the all-stainless steel vapor-chamber fin-tube radiator, because it results in the smaller weight increase. A least weight occurs for the vapor-chamber fin-tube geometries at specified final heat rejection because of the opposing variations of planform area and fin thickness as N_s/N is decreased. The effect of required increase in weight based on the full increase in planform area becomes greater than that of the reduction in fin thickness for the low values of N_s/N.

In another approach, the required increase in radiating area due to fin segment puncture can be assumed to be obtained by an increase in only the fin area, that is, by increasing fin L/R_o. In this case, the relative increase in radiator weight would be less than that shown in figure 10(a), because the fins constitute only around 15 to 25 percent of the total radiator weight. The corresponding increase in total radiator weight for this approach would then be the required increase in area multiplied by this weight fraction plus the weight of the additional header weight required (function of percent increase in L). Results for this case are shown plotted in figure 10(b). The resultant weight is less and is reached at a lower value of N_s/N than in the case of figure 10(a), because the effect of the area addition is relatively smaller.

In any event, it is clear that the two vapor-chamber fin cases (all stainless steel and stainless-steel-clad copper) at specified final heat rejection and temperature still yield a least specific weight substantially less than the central fin-tube geometry case (greater than a 36-percent reduction for the clad fin) and the double fin-tube geometry case (greater than a 20-percent reduction for the clad fin). The percent increase in radiator weight would be somewhat greater at lower values of tube nonpuncture probability because the fin constitutes a greater fraction of the total radiator weight.

Effect of meteoroid density. - The effect of the selected value of meteoroid particle density ρ_p on radiator least specific weight is shown in figure 11 over a range of values of $P(O)_t$ for the central and vapor-chamber fin-tube radiators. The plot is made for two values for ρ_p (0.2 g/cc, used throughout this report, and 0.5 g/cc). An increase in radiator specific weight from 11 to 16 percent is indicated for the central fin-tube radiator over the range of $P(O)_t$ values covered for an increase in ρ_p from 0.2 to 0.5 gram per cubic centimeter. For the vapor-chamber fin-tube radiator, the comparable increase in radiator specific weight is from 12 to 15 percent.

Effect of cycle component efficiency. - The previous results for least radiator weight were determined for a specific set of cycle component efficiencies (turbine efficiency η_t, generator efficiency η_g, and power availability factor K_p), and expressed as a fraction of the electrical power output Pe. In addition, a thermodynamic cycle efficiency η_{therm} is implied by the design temperature ratio T_R/T_M. For a fixed value of η_{therm} (fixed T_R/T_M), the specific heat-rejection rate will vary with component efficiencies according to the relation (ref. 2)

$$\frac{Q_{rej}}{Pe} \alpha \frac{1}{K_p \eta_g} \left(\frac{1}{\eta_t \eta_{therm}} - 1 \right) \tag{7}$$

If the geometric proportions of the radiator remained essentially constant as Q_{rej} varied, the specific weight of the radiator would vary at least directly with the heat-rejection rate. Inasmuch as variations in Q_{rej}/Pe with component efficiencies can be significant (see fig. 12), it is of interest to obtain some indication of the variation of radiator least specific weight as component efficiencies are varied.

Calculations of least specific weight based on specific initial heat rejection were made for several sets of values of η_g, η_t, and K_p (all other inputs held constant) for the central and vapor-chamber fin-tube radiators at $P(O)_t = 0.98$. The results of the calculations together with the respective values of heat-rejection rate are listed in table V.

TABLE V. - CALCULATED RADIATOR SPECIFIC WEIGHT FOR VARYING COMPONENT EFFICIENCIES

[Thermodynamic cycle efficiency, 0.281.]

Case	Efficiency		Power availability factor, K_p	Radiator heat-rejection rate, Q_{rej}		Central fin-tube		Vapor fin-tube	
	Turbine, η_t	Generator, η_g				Specific weight, W/Pe			
				Btu/hr	MW	lb/kW	kg/kW	lb/kW	kg/kW
Ideal	1.00	1.00	1.00	4.32×10^6	1.26	2.16	0.98	1.38	0.63
Calculated design results	.75	.90	.90	7.87×10^6	2.30	4.75	2.15	2.90	1.31
1	.70	.90	.72	10.65×10^6	3.11	7.14	3.24	4.29	1.96
2	.75	.82	.55	14.08×10^6	4.10	10.38	4.70	6.08	2.77
3	.50	.80	.55	23.30×10^6	6.80	20.30	9.21	11.76	5.36

Sizable increases in radiator least specific weight are therefore indicated for reduced values of cycle component efficiencies.

Table V shows that radiator specific weight increases at a greater rate than the increase in heat-rejection rate. It was found that for both radiator geometries, the least-weight variation could be closely approximated by a power function of the heat-rejection rate such that

$$\frac{\frac{W}{Pe}}{\left(\frac{W}{Pe}\right)_{id}} = \left[\frac{\frac{Q_{rej}}{Pe}}{\left(\frac{Q_{rej}}{Pe}\right)_{id}}\right]^{m} \tag{8}$$

where the subscript id refers to the ideal conditions of $\eta_g = \eta_t = K_p = 1.0$. The exponent m was 1.33 for the central fin-tube radiator and 1.26 for the vapor-chamber fin-tube radiator. The deduced variations of specific weight ratio with heat-rejection ratio given by equation (8) are plotted in figure 13. The points corresponding to the calculated results of the analysis ($\eta_t = 0.75$, $\eta_g = 0.90$, and $K_p = 0.90$) are shown in the figure.

The application of equation (8), with appropriate values of the exponent m for each type of radiator, yields estimates of the variation in radiator least specific weight for different values of cycle component efficiencies for the calculated radiator results. Although no specific comparison calculations are available, it is expected that the variation in least specific weight for the double fin-tube radiator will closely follow that of the central-fin-tube radiator.

The increase in specific weight for the central fin-tube radiator is indicated to be somewhat greater than for the vapor-chamber fin-tube radiator for the specific example investigated. If this is a consistent trend, the specific weight advantage of the vapor-chamber fin-tube radiator would be slightly more pronounced for cycles with reduced component efficiencies.

Effect of tube block sidewall thickness ratio. - As discussed in appendix C, a value of ratio of tube block sidewall thickness to maximum armor thickness δ_s/δ_a equal to 0.25 was selected for the vapor-chamber and double fin-tube geometries based on considerations of limited available impact data. However, if a larger thickness ratio is required to ensure nonpuncture, it is of interest to determine the resultant effect on radiator least specific weight. Calculations were accordingly made for the vapor-chamber fin radiator with $\delta_s/\delta_a = 0.75$, which is an extreme value. A comparison between the central and vapor-chamber fin-tube radiators over a range of tube nonpuncture probability is shown in figure 14. An increase in the value of δ_s/δ_a from 0.25 to 0.75 results in a 14- to 29-percent increase depending on the value of tube nonpuncture probability chosen. In any event, the vapor chamber fin-tube geometry maintains its weight superiority over the solid conducting central fin-tube radiator.

Radiator Geometry

Fin profile ratio. - The radiator fin profile ratio L/R_o obtained for minimum specific weight at each diameter for the vapor-chamber, double, and central fin-tube geome-

tries is shown plotted in figure 15. The L/R_o ratio associated with the vapor-chamber fin-tube geometries is larger than the values obtained for both the double fin-tube geometry and the central fin-tube geometry over the entire range of tube diameter investigated. The L/R_o ratio is relatively flat with the tube inside diameter for the three geometries at tube diameters greater than 3/8 inch (0.95 cm).

Planform area. - The radiator planform area is defined by the expression

$$A_p = 2R_o Z N_T \left(1 + \frac{L}{R_o}\right) \tag{9}$$

which, when divided by the powerplant electrical output in kilowatts, yields the radiator specific planform area. The specific planform area of the vapor-chamber, central, and double fin-tube geometries is shown plotted against tube inside diameter in figure 16 for the case of $P(O)_t = 0.98$. The two vapor-chamber fin-tube cases yield lower specific planform area over the entire range of tube inside diameters investigated. At the least specific weight condition, the two solid conducting fin geometries yield approximately the same specific planform area (0.80), while a somewhat smaller specific planform area of around 0.74 was obtained for the vapor-chamber fin-tube radiators.

The variation of radiator specific planform area at least weight is shown plotted against tube nonpuncture probability in figure 17. The curves indicate that the two vapor-chamber fin cases yield lower specific planform area over the entire range of tube nonpuncture probability investigated. However, the area reduction compared with the double fin geometry becomes quite small as the tube nonpuncture probability approaches 0.90.

For the case of specified final heat-rejection capability and temperature, the required increase in fin area will result in an increase in required planform area above the values given for the vapor chamber fin radiator in figures 16 and 17. If the increase in radiating area is approximated by an increase in the ratio of L/R_o for fixed Z, N_T, and R_o, the required radiator planform area will be given by the relation

$$\frac{A_{p,F}}{A_{p,I}} = \frac{1 + K\left(\frac{L}{R_o}\right)_I}{1 + \left(\frac{L}{R_o}\right)_I} \tag{10}$$

where the subscripts F and I refer, respectively, to the specified final conditions and specified initial conditions design, and K is the ratio of required radiating area for specified final conditions to that at specified initial conditions (taken as the inverse of Q_F/Q_I. Thus, for the case of least radiator specific weight at $P(O)_t = 0.98$ ($L/R_o = 5$ from

fig. 15), and $N_s/N = 0.65$ (fig. 10(a)), the required increase in radiator planform area will be around 5 percent for the stainless-steel clad fin case and around 10 percent for the all stainless-steel fin case. Such increases can readily negate the area reduction indicated for the vapor-chamber fin-tube radiator in figure 17.

Another factor to consider is that the planform area of the solid conducting fin geometries can be readily altered by changes in the design values of fin L/R_o ratio and conductance parameter N_c (which determines fin radiating efficiency). For the minimum weight condition at $P(O)_t = 0.98$, values of L/R_o are given in figure 15, and values of N_c are given in figure 18. However, significant reductions in both N_c and L/R_o from these minimum-weight values can be tolerated to achieve reduced planform areas with relatively small weight penalty, as indicated by the examples of figure 19. The principal contributor to this design tolerance is the relatively small fraction of the total radiator weight contributed by the fins.

It is thus seen that there is little, if any, reduction in radiator planform area achievable with the vapor-chamber fin-tube geometry compared with the central and double fin-tube geometries at or near the least-weight condition.

TABLE VI. - CALCULATED RADIATOR SPECIFIC PLANFORM AREA

Case	Efficiency		Power availability factor, K_p	Radiator heat-rejection rate, Q_{rej}		Central fin-tube		Vapor fin-tube	
	Turbine, η_t	Generator, η_g				Specific planform area, A_p/Pe			
				Btu/hr	MW	ft^2/kW	m^2/kW	ft^2/kW	m^2/kW
Ideal	1.00	1.00	1.00	4.32×10^6	1.26	0.446	0.0415	0.404	0.0376
Calculated design results	.75	.90	.90	7.87×10^6	2.30	.815	.0758	.738	.0686
1	.70	.90	.72	10.65×10^6	3.11	1.118	.1040	.997	.0927
2	.75	.82	.55	14.08×10^6	4.10	1.460	.1358	1.334	.1240
3	.50	.80	.55	23.30×10^6	6.80	2.410	.2240	2.230	.2070

The effect of cycle component efficiencies on the magnitude of the specific planform area for the least-weight condition was also investigated. Calculated specific planform area at the least-specific-weight condition for the vapor-chamber and central fin-tube radiators for $P(O)_t = 0.98$ is tabulated in table VI for several sets of component efficiencies. The percentage increase in specific planform area was indicated to be identical to the percentage increase in heat-rejection rate in both cases, such that

$$\frac{\frac{A_p}{Pe}}{\left(\frac{A_p}{Pe}\right)_{id}} = \frac{\frac{Q_{rej}}{Pe}}{\left(\frac{Q_{rej}}{Pe}\right)_{id}} \tag{11}$$

Thus, the ratio of planform area to heat-rejection rate is a constant value.

Tube armor thickness. - Figure 20 shows a plot of tube armor thickness δ_a against tube inside diameter for the three geometries investigated. The vapor-chamber fin-tube has the smallest values of δ_a because of the reduced tube vulnerable area which results from the high thermal effectiveness of this geometry. The central fin-tube configuration has the largest armor thickness because its vulnerable area is based on the full outer surface of a round tube, whereas the vulnerable area of both the double and vapor-chamber fin-tube geometries are based on the projected area of the tube block (which is always less).

There was no difference in armor thickness for the all stainless steel and stainless-steel-clad copper fin-tube radiators.

Fin thickness. - Comparison of the fin thickness obtained for the three fin-tube configurations at minimum weight is shown in figure 21. The fin thickness of the vapor-chamber fin-tube radiator was constant with tube inner diameter at a value of around 0.010 inch (0.25 cm). Vapor-chamber fin thickness is determined solely from meteoroid protection considerations, which in this case did not vary with tube inner diameter.

The fin thickness obtained for the central fin radiator $2t$ is considerably larger (0.020 to 0.050 in. or 0.051 to 0.127 cm) than the fin thickness t associated with the double fin-tube geometry (from t = 0.010 to 0.018 in. or 0.025 to 0.046 cm) or vapor-chamber fin-tube geometry (t = 0.010 to 0.012 in. or 0.025 to 0.030 cm). Both solid conducting fin-tube radiators exhibited increasing fin thickness with increasing tube inner diameter.

In order to increase the structural integrity of the double fin-tube geometry, the fin thickness can be increased by designing it with a smaller value of conductance parameter N_c than the value at least-weight conditions. For example, the fin thickness of a double fin-tube radiator can be increased from 0.012 to 0.022 inch (0.033 to 0.056 cm) with only a 5-percent penalty in weight (conditions of fig. 19(b)). This required a change in conductance parameter N_c from 0.55 to 0.27.

Number of tubes. - The number of radiator tubes for the three geometries decreased substantially as the tube inside diameter increased (fig. 22). In general, the vapor-chamber fin-tube had the smallest number of tubes for any specific choice of tube inside diameter. Comparison of the number of tubes for the three radiators at the diameter corresponding to least specific weight (see fig. 7), indicated the vapor-chamber fin-tube

radiators required only 135 tubes at a diameter of 0.53 inch (1.35 cm), whereas the central fin has approximately 240 tubes at a diameter of 0.47 inch (1.20 cm) and the double fin-tube had 450 tubes at a diameter of 0.31 in.) (0.79 cm). Further advantage of the vapor-chamber fin-tube radiator is that the number of tubes can be reduced even further by going to tube diameters larger than that required for least weight without a large penalty in W/Pe (fig. 7).

Panel aspect ratio. - Radiator panel aspect ratio w/Z (fig. 1) is shown plotted for the three fin-tube geometries in figure 23 against tube inside diameter. These values of aspect ratio for the individual panels as defined in figure 1 are also the overall values of aspect ratio for the entire radiator. A pronounced decrease in aspect ratio occurs with increasing tube inside diameter. For the least-weight condition, the radiator aspect ratios for the vapor-chamber fin-, central fin-, and double fin-tube geometries are, respectively, 2, 3.2, and 7.3.

According to figure 23, if the radiator installation requires relatively low values of aspect ratio (i.e., less than 1.5), designs with tube inside diameters greater than 5/8 inch (1.59 cm) will be required for $P(O)_t = 0.98$. For such tube diameters, the double fin radiator will have the greatest weight and planform area (figs. 7 and 16), while the vapor-chamber fin-tube radiator will have the least weight and area. For a radiator aspect ratio of one (D_i = 3/4 in. or 1.90 cm), the vapor-chamber fin-tube radiator specific weight is 3.10 pounds per kilowatt (1.40 kg/kW) against 5.13 pounds per kilowatt (2.33 kg/kW) for the central fin radiator, and 5.40 pounds per kilowatt (2.46 kg/kW) for the double fin radiator. The respective specific planform areas are 0.785, 0.865, and 0.985 square foot per kilowatt (0.0725, 0.0805, and 0.0915 m^2/kW).

SUMMARY OF RESULTS

A comparison of representative vapor-chamber fin-tube radiators with either stainless-steel-clad copper or all-stainless-steel fins and solid-conducting central and double fin-tube radiators using stainless-steel-clad copper fins for the sample case of a 500-kilowatt, high-temperature Rankine cycle revealed the following principal results:

1. The vapor-chamber fin geometry yielded a radiator least specific weight, at specified initial heat rejection, 28 to 45 percent less than the central fin and 13 to 29 percent less than the double fin geometries over the range of tube nonpuncture probability $P(O)_t$ from 0.90 to 0.995. At $P(O)_t = 0.98$, the least specific weights were 4.75, 3.85, and 2.90 pounds per kilowatt (2.15, 1.75, and 1.31 kg/kW), respectively, for the central, double, and vapor-chamber fin-tube radiators. For the vapor-chamber fin-tube radiator, the use of all-stainless-steel fins or stainless-steel-clad copper fins varied the radiator weight by only 2 percent.

2. For the design condition of specified heat rejection and temperature at the end of

the design lifetime of the radiator, the relative least-specific-weight advantage of the vapor-chamber fin-tube radiator was reduced because of thermal radiation degradation. Compared with the case of specified initial heat rejection at $P(O)_t = 0.98$, the vapor-chamber radiator was 3 to 11 percent heavier for all-stainless-steel fins and 2 to 6 percent heavier with stainless-steel-clad copper fins, depending on the method of calculating the thermal degradation.

3. At least specific weight, the specific planform area of the vapor-chamber fin-tube geometry was from 6 to 8 percent less than the central fin-tube geometry, and from 2 to 12 percent less than the double fin-tube geometry over the range of tube nonpenetration probabilities investigated (0.90 to 0.995). Values of specific planform area at $P(O)_t = 0.98$ were 0.814, 0.800, and 0.740 square foot per kilowatt (0.0755, 0.0744, and 0.0687 m^2/kW), respectively, for the central, double, and vapor-chamber fin-tube radiators. However, these differences in planform area can readily be equalized by designing the conducting fin radiators for reduced values of fin profile ratio with only a modest increase in specific weight ($\sim$2 percent).

4. An approximate correction for variation of radiator specific weight with increased radiator heat-rejection rate due to reduced cycle component efficiencies showed that radiator least specific weight increased exponentially with heat-rejection rate. Least weight for the central fin-tube radiator increased at a slightly greater rate than for the vapor-chamber fin-tube radiator.

5. Radiator specific planform area at least specific weight increased directly with increased radiator heat-rejection rate, which resulted from reduced cycle component efficiencies for all fin-tube geometries.

6. For the least specific weight condition at $P(O)_t = 0.98$, the tube inside diameter was 0.31, 0.47, and 0.53 inch (0.79, 1.19, and 1.34 cm), respectively, for the double, central, and vapor-chamber fin-tube radiators. Number of tubes, respectively, was 450, 240, and 135, and radiator panel aspect ratio was 7.3, 3.2, and 1.9.

7. Except for a relatively small effect on required planform area for specified final heat rejection, the choice of vapor-chamber fin material had negligible effect on the geometric characteristics of the vapor-chamber fin-tube radiators.

8. For values of tube inside diameter greater than those for radiator least specific weight, the relative weight and planform area increases remained about the same for the vapor-chamber and central fin-tube radiators (around 8 percent for area and 18 percent for weight at 1-in. (2.54-cm) diameter). However, these values increased markedly for the double fin-tube radiator as tube inside diameter was increased (around 25 percent for area, and 65 percent for weight at 1-in. (2.54-cm) diameter).

CONCLUDING REMARKS

The analytical study of high-temperature Rankine cycle direct-condensing radiators for different fin-tube geometry has shown that there is basically little difference in achievable specific planform area for the three geometries considered. However, radiator least specific weight can be substantially different, with the vapor-chamber fin-tube radiator showing least weight in all cases. The magnitude of the weight differences will depend to a large extent on the specific input values chosen for the cycle and radiator components and on the comparison basis. Thus, an evaluation of the potential merit of a particular radiator fin-tube geometry should be based on a detailed weight and geometry analysis covering a wide range of input variables pertinent to the specific design application. At the same time, consideration should also be given to the possible complexities and unknowns involved in a particular geometric configuration which are not covered in the weight analysis. In the case of the vapor-chamber fin-tube radiator, such factors as the internal mechanics and thermodynamics of the capillary flow and possible structural complications involved in fin compartment sealing and buckling strength should be considered.

Lewis Research Center,
National Aeronautics and Space Administration,
Cleveland, Ohio, November 2, 1967,
120-27-04-36-22.

APPENDIX A

SYMBOLS

A_p	radiator planform area, sq ft; m^2
A_{seg}	fin segment planform area, sq ft; m^2
A_v	vulnerable area, sq ft; m^2
a_f	fin perforation factor
a_t	tube incipient spall factor
b	vapor-chamber fin segment width, ft; m
C	constant in eqs. (4) and (5)
D	diameter, ft; m
E	Young's modulus of target material, lb/sq ft; N/m^2
g	gravitational constant, (lb force)(sec^2)/(lb mass)(ft); (N)(sec^2)/(kg)(m)
K	ratio of required radiating area for specified final conditions to that at specified initial conditions
K_p	fraction of generator output available as power output or power availability factor
k	thermal conductivity, Btu/(ft)(hr)(^oF); W/(cm)(^oK)
L	half-length of fin between tubes (fig. 2), ft; m
L/R_o	fin profile ratio
l	half-length of fin between tubes, equal to $L + \left(1 - \frac{\delta_s}{\delta_a}\right)\delta_a$, ft; m
l/R_b	vapor-chamber fin profile ratio
m	power exponent
N	number of fin segments
N_c	fin conductance parameter, $\frac{\sigma T_b^3 l^2}{kt}$
N_s	number of fin segments not punctured in given time
N_T	number of radiator tubes

P	cycle fluid pressure, lb/sq ft; N/m^2
Pe	electrical power output, kW
P(O)	probability of no critical damage to radiator tubes, headers, or fin segment
Q	heat rejection rate, Btu/hr; W
Q_{rej}	radiator heat rejection rate, Btu/hr; W
R_b	distance from tube sidewall to tube centerline, $R_b = R_o - \left(1 - \frac{\delta_s}{\delta_a}\right)\delta_a$, ft; m
R_o	tube outside radius, ft; m
S	overall fin nonpenetration probability
T_b	temperature of tube block outer surface, ^oR; ^oK
T_M	maximum cycle temperature, ^oR; ^oK
T_R	radiator inlet total temperature, ^oR; ^oK
t	fin thickness (see fig. 2), in.; cm
V	velocity, ft/sec; m/sec
W	weight, lb; kg
w	panel width, ft; m
x	position on fin
y	coordinate
Z	tube length, ft; m
α, β	constants in penetration formula
γ	material cratering coefficient
δ_a	tube block armor protection thickness, in.; cm
δ_s	tube block sidewall thickness, in.; cm
η_g	generator efficiency
η_t	turbine efficiency
η_{therm}	thermodynamic cycle efficiency
ρ	density, lb/cu ft; kg/m^3
τ	mission time, days

Subscripts:

a	tube armor
cu	copper
eff	effective
F	specified final conditions
f	fin
I	specified initial conditions
i	inside
id	ideal case
o	outside
p	particle
ss	stainless steel
t	tube

APPENDIX B

CLAD FIN CONSIDERATIONS

Vapor-Chamber Fin-Tube Geometry

The effects of changes in factors such as the copper modulus of elasticity E_{cu} and stainless-steel-clad-to-copper thickness ratio t_{ss}/t_{cu} on the vapor-chamber fin-tube geometry were investigated. The results allowed the choice of a typical case that was used for comparison with other radiator geometries.

Values of the minima of curves similar to those of figure 5 obtained for variations of copper modulus of elasticity indicated less than a 4-percent variation in radiator specific weight when the copper modulus was varied from 0.0288×10^{10} to 0.144×10^{10} pounds per square foot (1.434×10^{10} to 7.17×10^{10} N/m^2). This comparison was obtained for $P(O)_t$ = 0.98 and a tube inside diameter of 1/2 inch (1.27 cm) (near least-weight condition). This small variation in W/Pe occurred because the fin thickness is a function of the 1/3 power of the composite modulus of the material (eq. (5)). In view of the relatively small variation in radiator weight over the range of modulus values covered, the middle E_{cu} value of 0.0576×10^{10} pounds per square foot (2.868×10^{10} N/m^2) (table I) was selected for the comparison calculations.

The variation of fin stainless-steel-to-copper thickness ratio t_{ss}/t_{cu} from 0.15 to 0.40 resulted in less than a 3-percent variation in radiator specific weight. However, the variation in t_{ss}/t_{cu} produced significant variations in the thickness of the stainless-steel clad. The calculated variation of the thickness of the stainless-steel clad is shown in figure 24(a) against stainless-steel-clad to copper thickness ratio t_{ss}/t_{cu} for several values of fin segment planform area A_{seg}. The general observation is that a stainless-steel-to-copper thickness ratio less than 0.40 is not desirable because the clad thickness would be less than around 0.0015 inch (0.0038 cm), which may be a lower practical limit. On the basis of the proceding variations, a value of t_{ss}/t_{cu} of 0.40 was selected for the weight and geometry comparisons.

Solid Conducting Fin Geometries

The fin dimensions and resultant weight for the central and double solid conducting fin-tube radiators are based primarily on the thermal conductivity of the fin material. Variation of the stainless-steel-to-copper thickness ratio from 0.15 to 0.40, which determines the thermal conductivity of the composite, resulted in less than a 3-percent increase in radiator specific weight for the central fin-tube geometry at least-weight con-

ditions. The double fin-tube geometry had a 4-percent increase in radiator specific weight for the same variation in t_{ss}/t_{cu}. The stainless-steel clad thickness at minimum specific weight for the two solid conducting fin radiators is plotted against t_{ss}/t_{cu} in figure 24(b). For the previous criterion of a minimum stainless-steel clad thickness of around 0.0015 inch (0.0038 cm), it is seen that a thickness ratio t_{ss}/t_{cu} of 0.40 is also required for the double fin geometry. Although a clad thickness ratio of 0.15 could be used for the central fin-tube radiator (with a 3-percent reduction in specific weight), for simplicity, a fixed common value of 0.40 for thickness ratio was used in the comparison calculations. The value of t_{ss} for the central fin-tube geometry is over twice that obtained for the double fin-tube geometry because the single fin associated with the central fin is twice the thickness of a single fin of the double fin-tube geometry.

APPENDIX C

VAPOR-CHAMBER FIN-TUBE RADIATOR INPUT VARIABLES

Because of the numerous input variables required to determine the heat-transfer characteristics of the vapor chamber and the geometry and weight of the radiator, it was necessary to conduct an initial investigation of the major influencing parameters. The heat-transfer characteristics of the vapor-chamber (which in reality depend on the internal heat-transfer mechanism, the choice of internal transfer fluid, and the choice of capillary medium) are prescribed by the control parameters of boiling and condensing heat-transfer coefficients.

The geometry and weight of a vapor-chamber fin-tube radiator are affected by the fin segment planform area A_{seg}, the fin segment aspect ratio $2\ell/b$, the ratio of surviving to total fin segments N_s/N, and the number of fin segments required N. Because the fin wall thickness is determined from meteoroid considerations; the surface area, number of segments, N_s/N ratio, and the properties of the fin material dictate the weight for a choice of overall fin nonpenetration probability S. The segment aspect ratio sets the rectangular shape of the fin outer surface and is a consideration in determining the structural capability of the chamber.

From meteoroid considerations, the fin wall thickness and the weight increase as the fin segment planform area increases. For the composite fin material, an increase in A_{seg} from 20 to 50 square inches (129 to 323 cm^2) results in only a 3-percent increase in radiator specific weight at a value of $S = 0.90$, $N_s/N = 0.75$, and a tube $P(O)_t = 0.98$, as shown in figure 25. The vapor-chamber fin geometry associated with the variation in segment planform area is shown for the sample case on figures 26 and 27. Figure 26 shows the variation in the number of fin chamber segments with fin segment planform area for two choices of tube inside diameter that yield near least weight. The variation of fin segment aspect ratio $2\ell/b$ with A_{seg} is shown in figure 27. Both the number of segments and the aspect ratio decrease as the segment planform area increases. These results were essentially the same for the all-stainless-steel vapor-chamber fins.

In general, the selection of a representative value of segment area A_{seg} for use in radiators is a compromise among the factors of reduced weight (low A_{seg}), reduced number of segments (high A_{seg}) and vapor-chamber aspect ratio (structural consideration), as illustrated in the variations of figures 25 to 27. Results of unpublished tests of square vapor-chamber fin plates of stainless steel and stainless-steel-clad copper with a planform area of 25 square inches (63.5 cm^2) indicated no serious structural problem when the test plates were subjected to a pressure differential of 1 atmosphere (1×10^5 N/m^2). Close comparison between experimental maximum deflections and values predicted from available applicable theory were also observed. For the representative vapor-

chamber fin configuration used in the comparison analysis, a compromise value of A_{seg} = 30 square inches (193.5 cm^2) was selected.

Another parameter that has a large effect on radiator weight is the choice of tube block sidewall to maximum armor thickness ratio δ_s/δ_a. Inasmuch as no experimental hypervelocity impact data were available for the specific geometric configuration of the block vapor fin-tube cross section, a representative value for the ratio δ_s/δ_a was deduced from related data. Reference 11 presents impact data for stainless-steel tubes shielded by a flat, 0.018-in. (0.045-cm) thick stainless-steel bumper displaced from the surface of the tube by around 0.60 inch (1.52 cm). Comparison of results from these bumpered tubes and unprotected tubes when hit by the same normally-impacting projectiles showed that the tube wall thickness required to produce a given type of inner-surface damage in the bumpered case was of the order of 0.2 the thickness observed in the comparable unprotected tube. The block fin-tube geometry departs from the above configuration in that it contains an attached bumper which involves only oblique secondary impacts and for the most part also oblique primary impacts. However, consideration of the oblique and normal impact phenomena and the geometries involved in the two cases lead to the judgement that the required wall thickness for the block geometry would be at least comparable to that required in the displaced bumper case. Accordingly, a representative value of sidewall thickness ratio for the calculations was selected as $\delta_s/\delta_a = 0.25$.

REFERENCES

1. Haller, Henry C.; Wesling, Gordon C.; and Lieblein, Seymour: Heat-Rejection and Weight Characteristics of Fin-Tube Space Radiators with Tapered Fins. NASA TN D-2168, 1964.

2. Krebs, Richard P.; Haller, Henry C.; and Auer, Bruce M.: Analysis and Design Procedures for a Flat, Direct-Condensing, Central Finned-Tube Radiator. NASA TN D-2474, 1964.

3. Saule, Arthur V.; Krebs, Richard P.; and Auer, Bruce M.: Design Analysis and General Characteristics of Flat-Plate Central-Fin-Tube Sensible-Heat Space Radiators. NASA TN D-2839, 1965.

4. Haller, Henry C.: Comparison of Heat-Rejection and Weight Characteristics of Several Radiator Fin-Tube Configurations. NASA TN D-2385, 1964.

5. Haller, Henry C.: Analysis of a Double Fin-Tube Flat Condenser-Radiator and Comparison with a Central Fin-Tube Radiator. NASA TN D-2558, 1964.

6. Haller, Henry C.; Lieblein, Seymour; and Lindow, Bruce G.: Analysis and Evaluation of a Vapor-Chamber Fin-Tube Radiator for High-Power Rankine Cycles. NASA TN D-2836, 1965.

7. Haller, Henry C.; Lindow, Bruce G.; and Auer, Bruce M.: Analysis of Low-Temperature Direct-Condensing Vapor-Chamber Fin and Conducting Fin Radiators. NASA TN D-3103, 1965.

8. Loeffler, Irvin J.; Clough, Nestor; and Lieblein, Seymour: Recent Developments in Meteoroid Protection for Space Power Systems. Space Power Systems Engineering. G. C. Szego and J. E. Taylor, eds., Academic Press, 1966, pp. 503-523.

9. Stockman, Norbert O.; and Bittner, Edward C.: Two-Dimensional Heat Transfer in Radiating Stainless-Steel-Clad Copper Fins. NASA TN D-3102, 1965.

10. Clough, Nestor; McMillan, A. R.; and Lieblein, Seymour: Dimple, Spall, and Perforation Characteristics of Aluminum, Columbium, and Steel Plates under Hypervelocity Impact. NASA TN D-3468, 1966.

11. Clough, Nestor; McMillan, A. R.; and Lieblein, Seymour: Material and Geometry Aspects of Meteoroid Armor Protection for Space Radiator Tubes. AIAA and and ASME Seventh Structures and Materials Conference, Cocoa Beach, Fla., Apr. 18-20, 1966. AIAA, 1966, pp. 459-466.

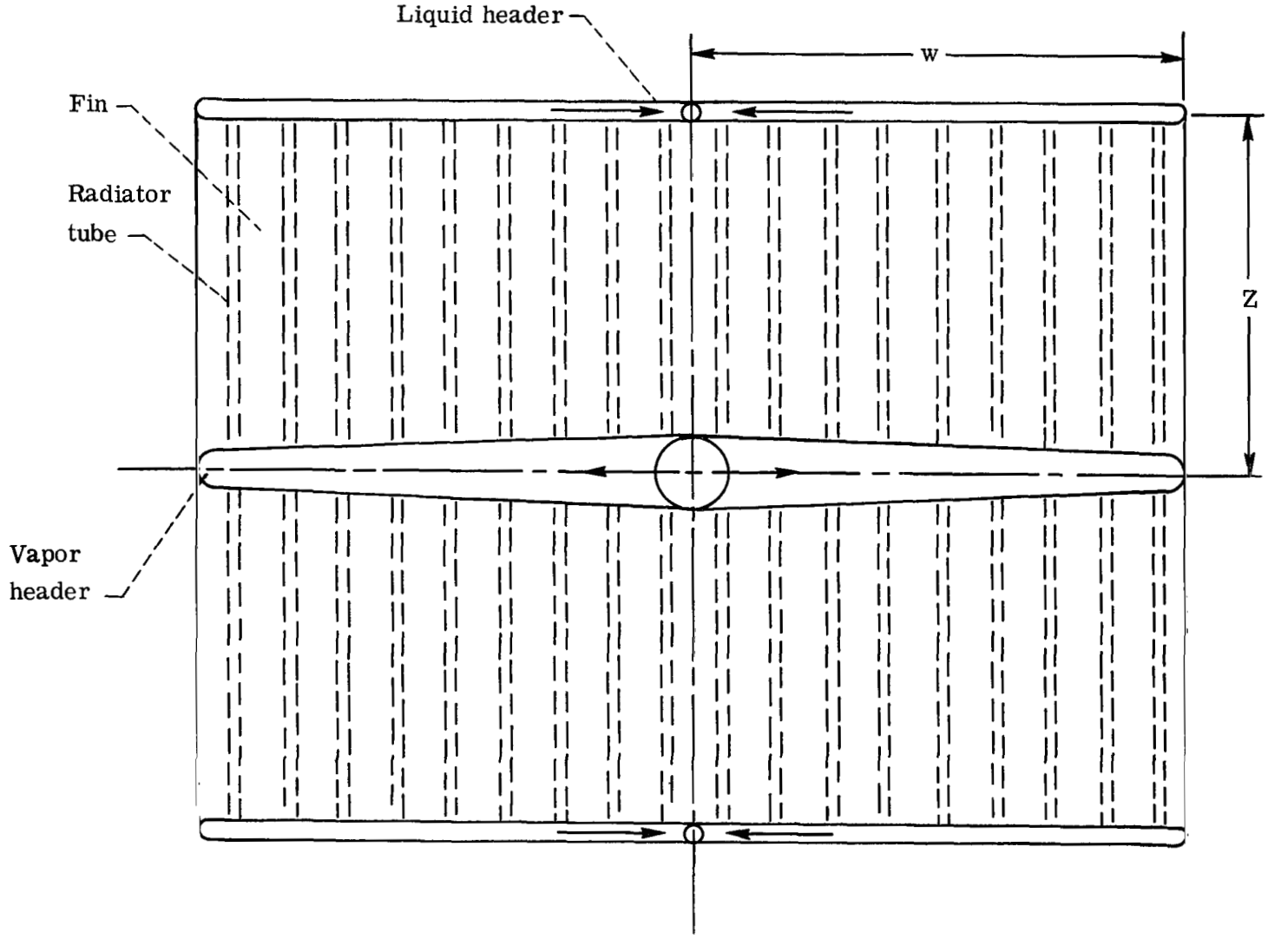

Figure 1. - Flat-plate radiator configuration.

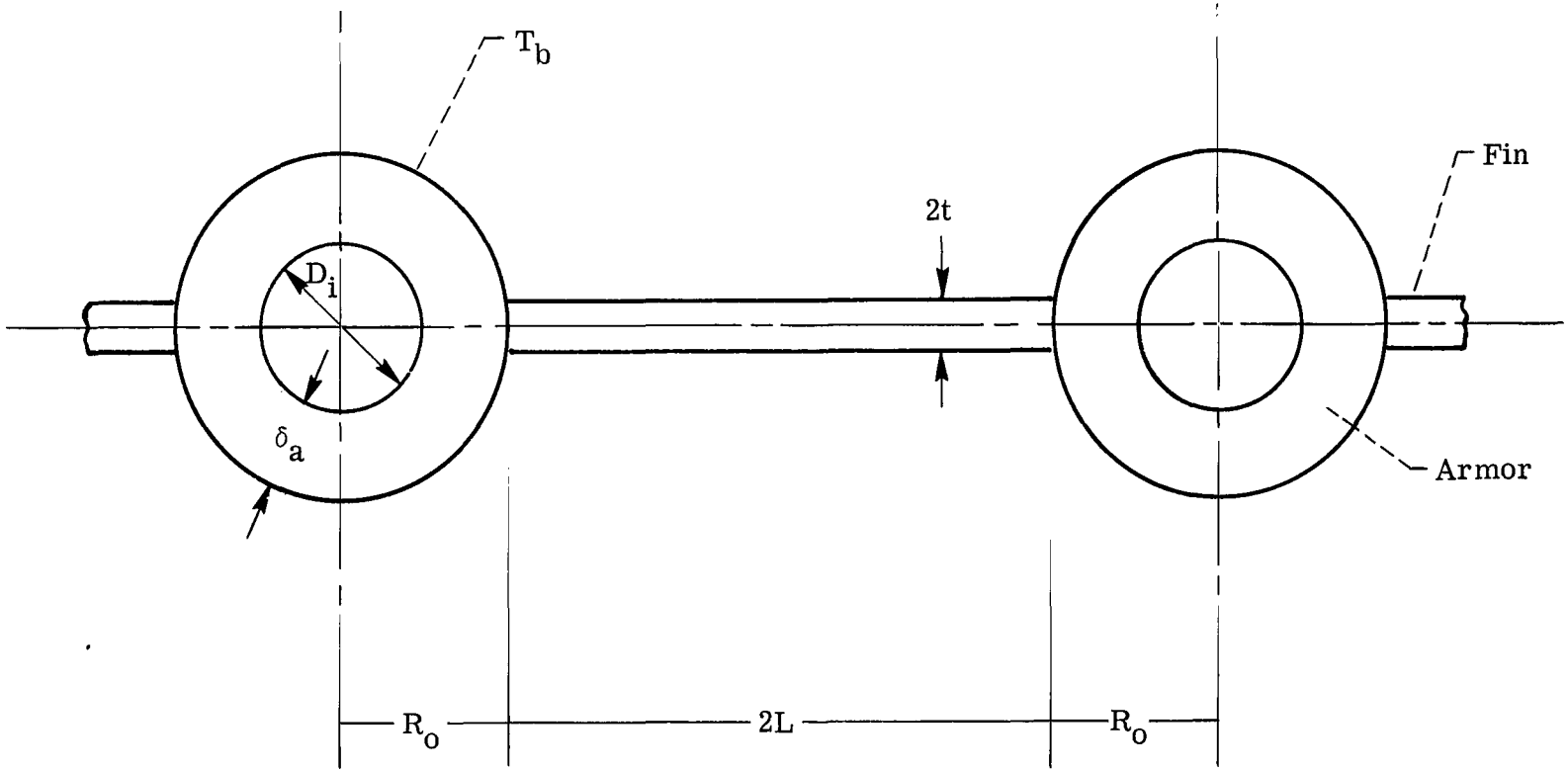

(a) Central fin-tube geometry.

Figure 2. - Radiator fin-tube configuration cross sections.

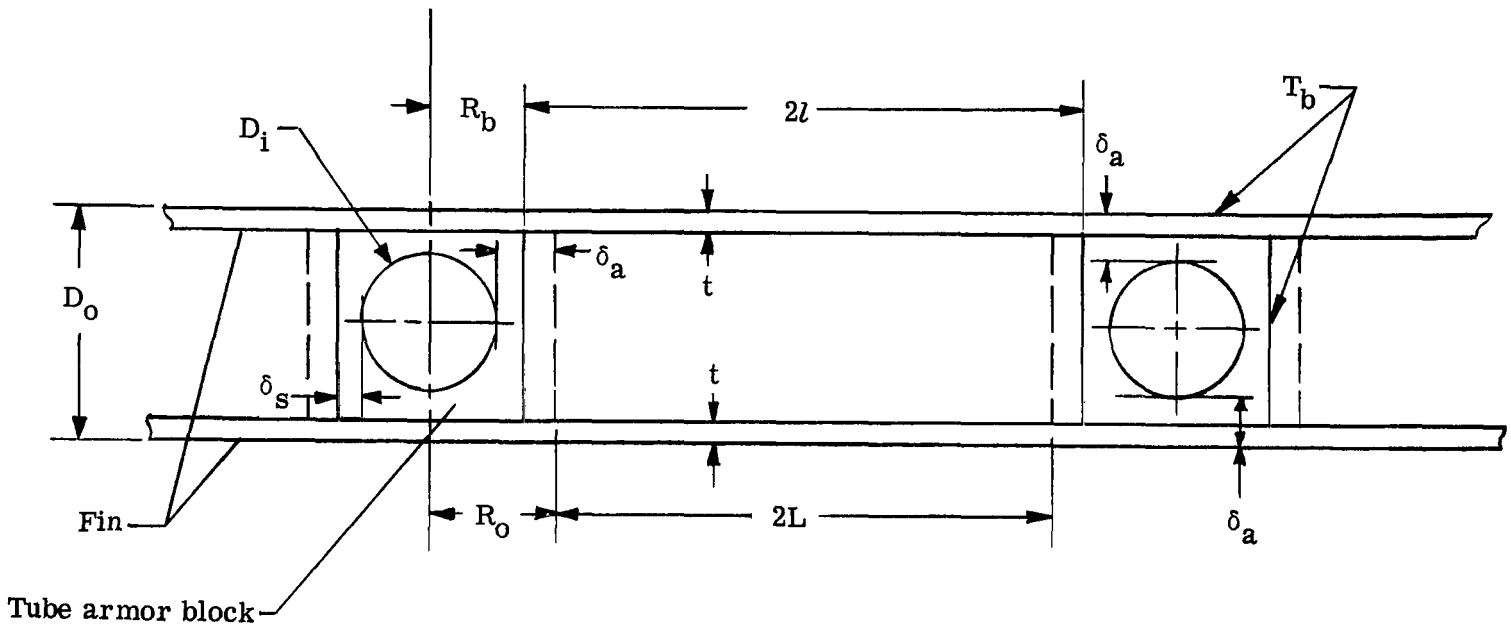

(b) Double fin-tube geometry with variable tube block sidewall thickness.

Figure 2. - Continued.

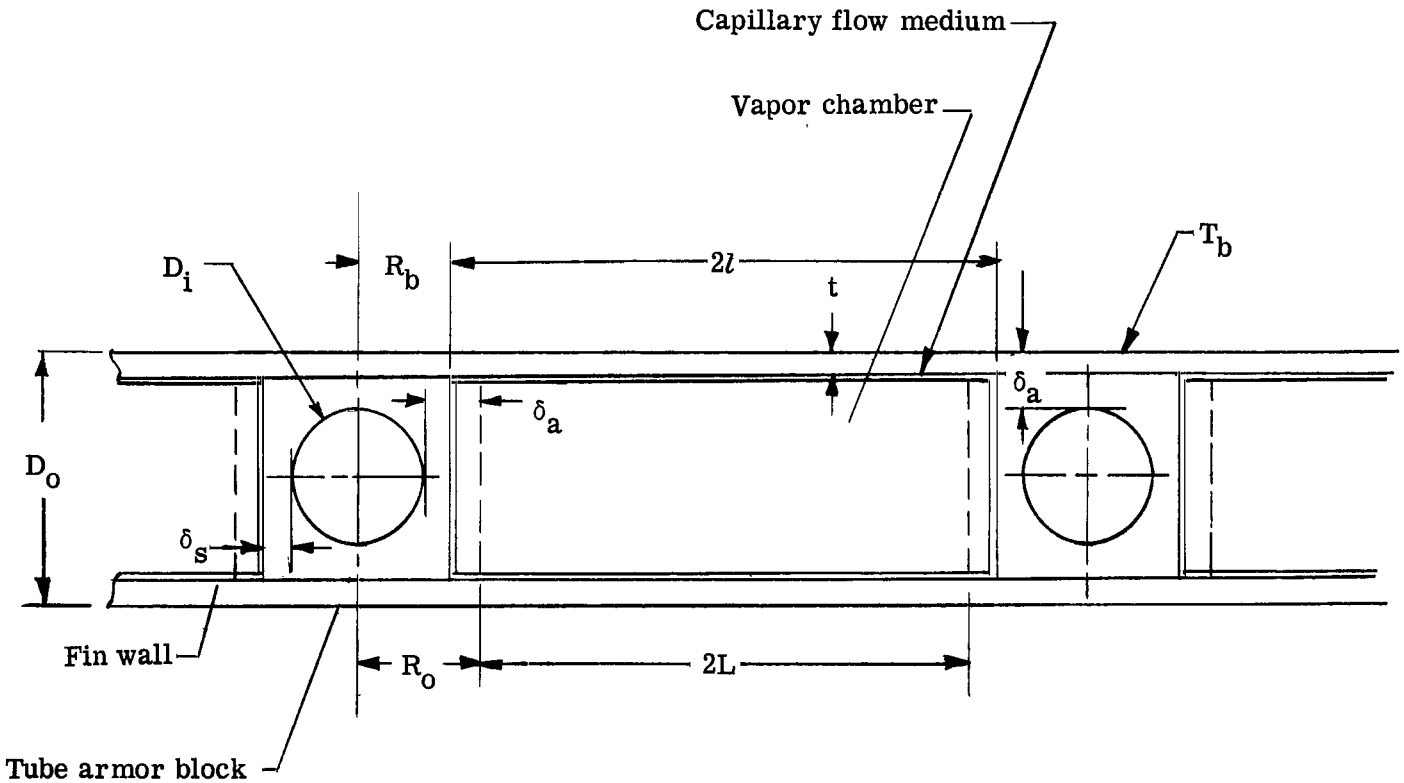

(c) **Block-vapor-chamber fin-tube geometry.**

Figure 2. - Concluded.

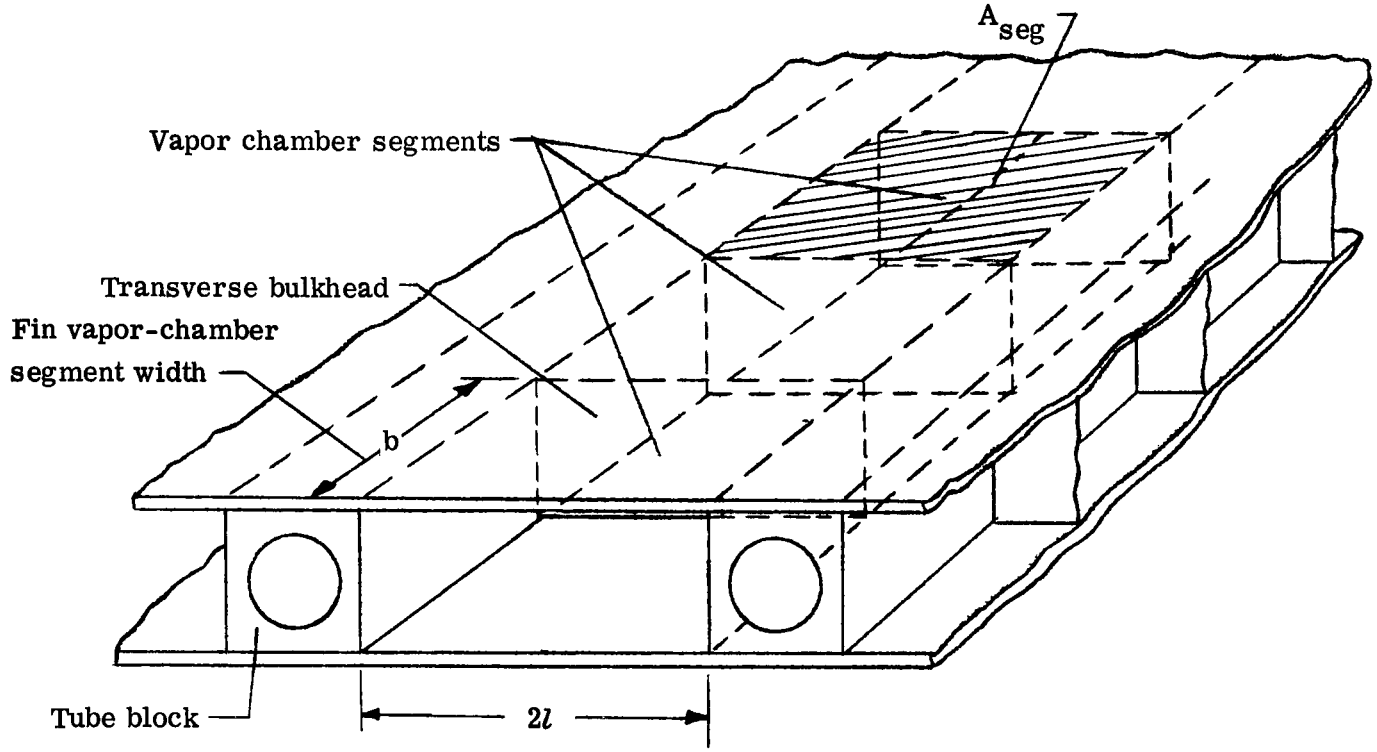

Figure 3. - Vapor-chamber fin-tube schematic.

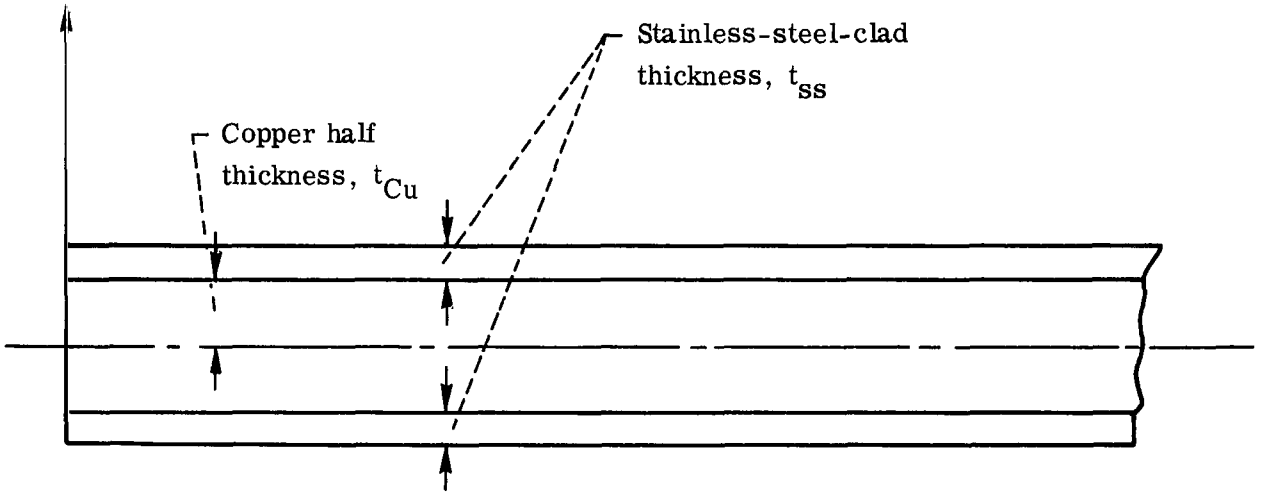

Figure 4. - Cross section of stainless-steel-clad copper fin.

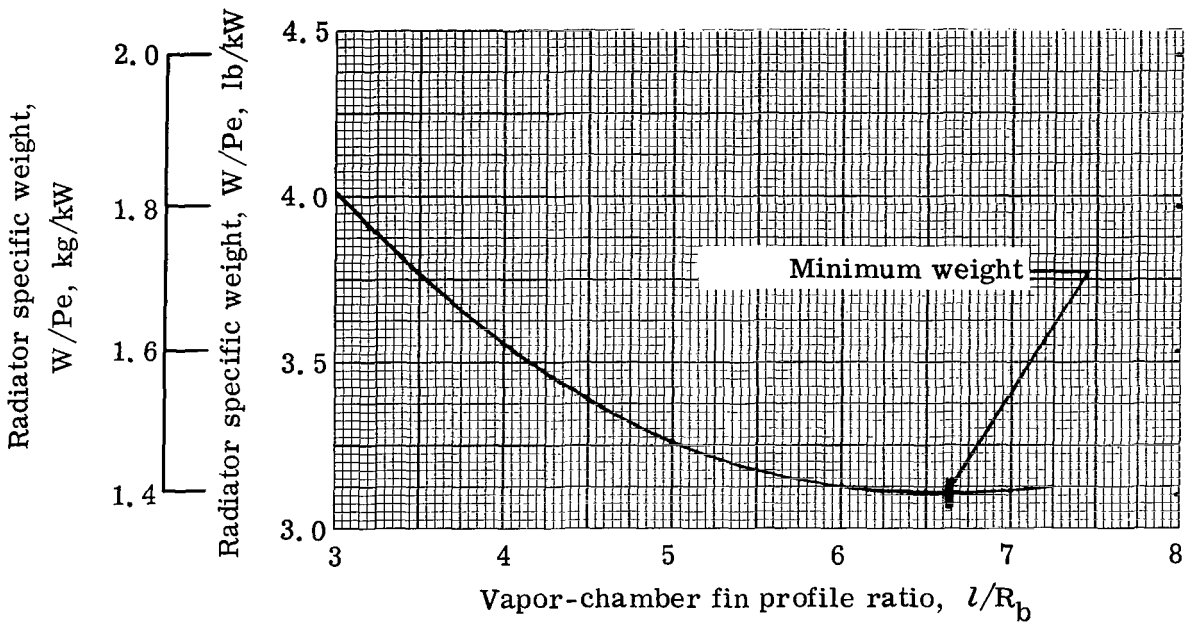

Figure 5. - Variation of radiator specific weight with vapor-chamber fin profile ratio. Stainless-steel clad to copper thickness ratio, 0.40; percent surviving fin segments, 75; vapor-chamber fin segment planform area, 30 square inches (193.5 cm^2); tube inside diameter, 3/4 inch (1.904 cm); tube nonpuncture probability, 0.98.

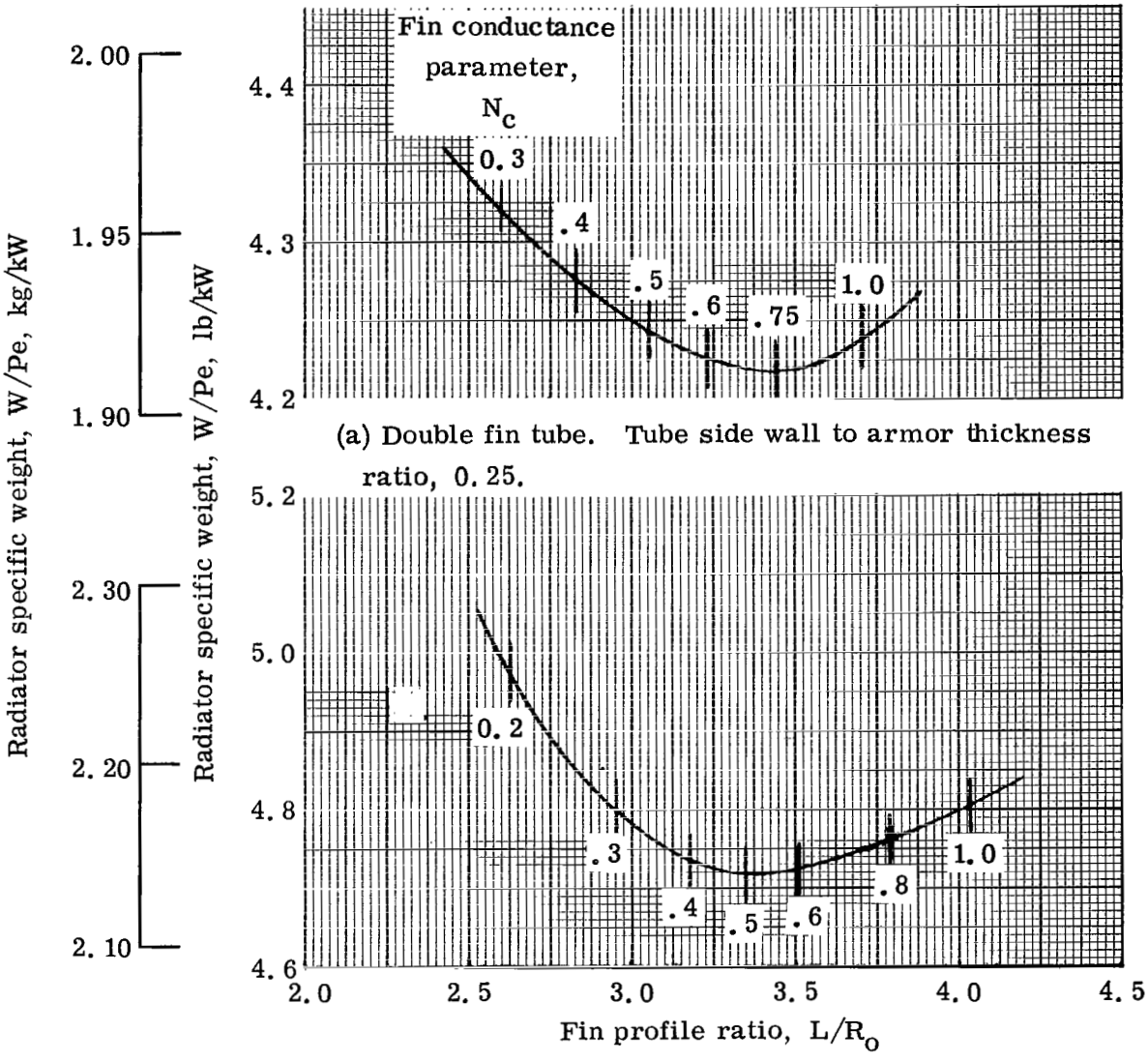

(a) Double fin tube. Tube side wall to armor thickness ratio, 0.25.

(b) Central fin tube.

Figure 6. - Variation of radiator specific weight with fin profile ratio. Tube nonpuncture probability, 0.98; tube inside diameter, 1/2 inch (1.27 cm); stainless-steel-clad to copper thickness ratio, 0.40.

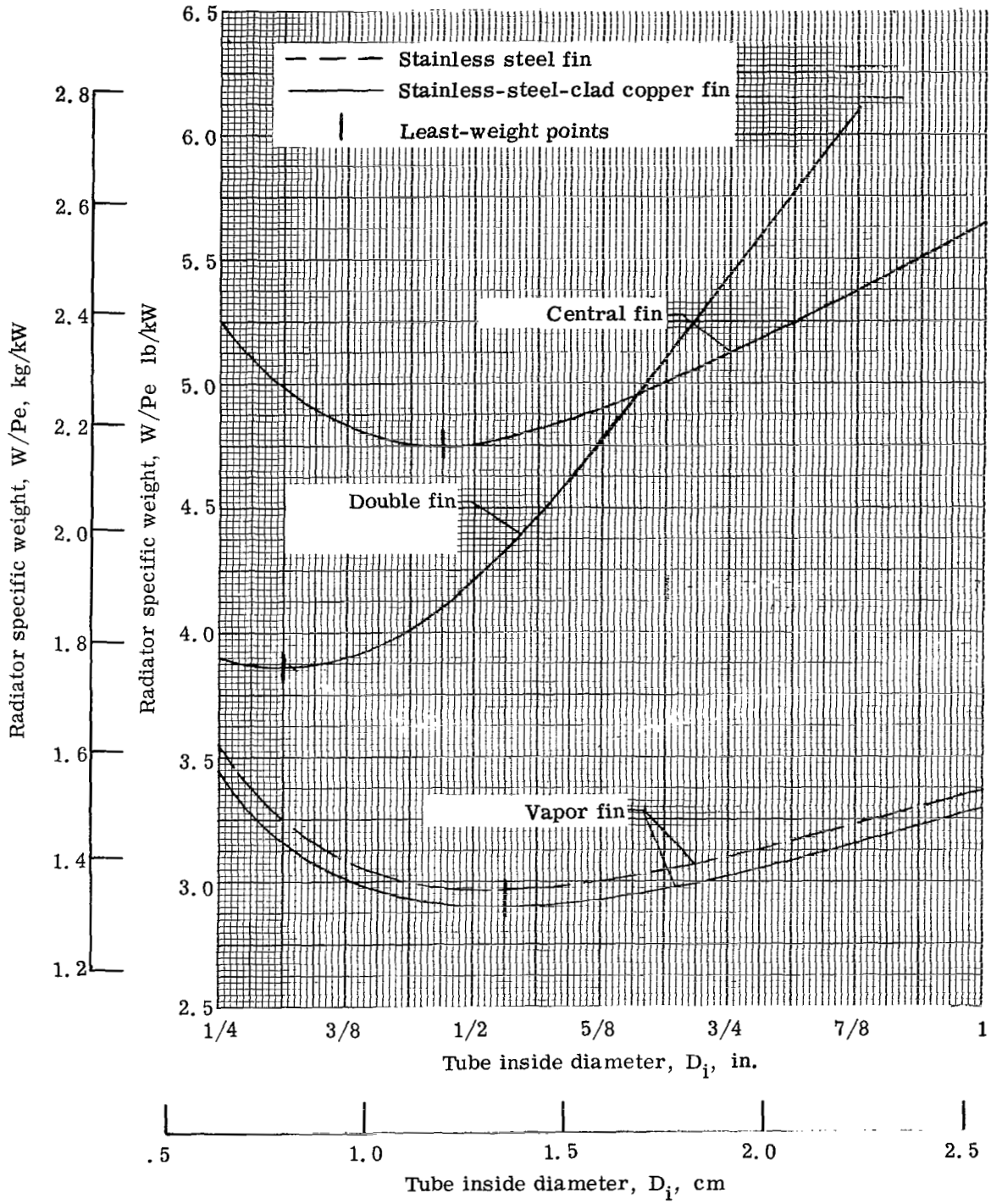

Figure 7. - Comparison of minimum radiator specific weight for vapor-chamber, central, and double fin-tube geometries. Tube nonpuncture probability, 0.98; percent surviving fin segments, 75; vapor-chamber fin segment planform area, 30 square inches (198.5 cm^2); tube block sidewall thickness ratio, 0.25.

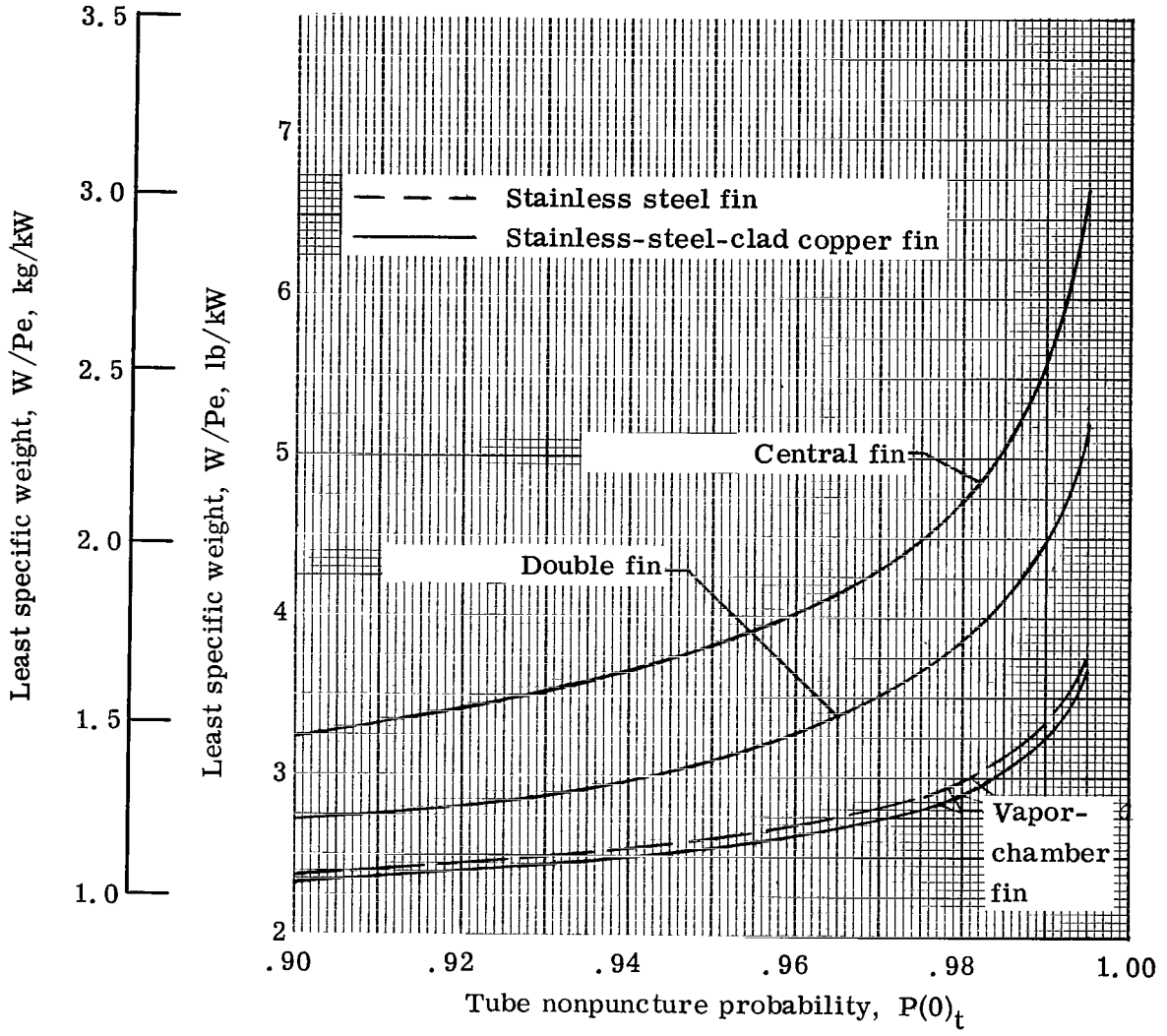

Figure 8. - Variation of least specific weight with tube nonpuncture probability. Tube block sidewall thickness ratio, 0.25; stainless-steel clad to copper thickness ratio, 0.40; percent surviving fin segments, 75; fin segment planform area, 30 square inches (193.5 cm^2).

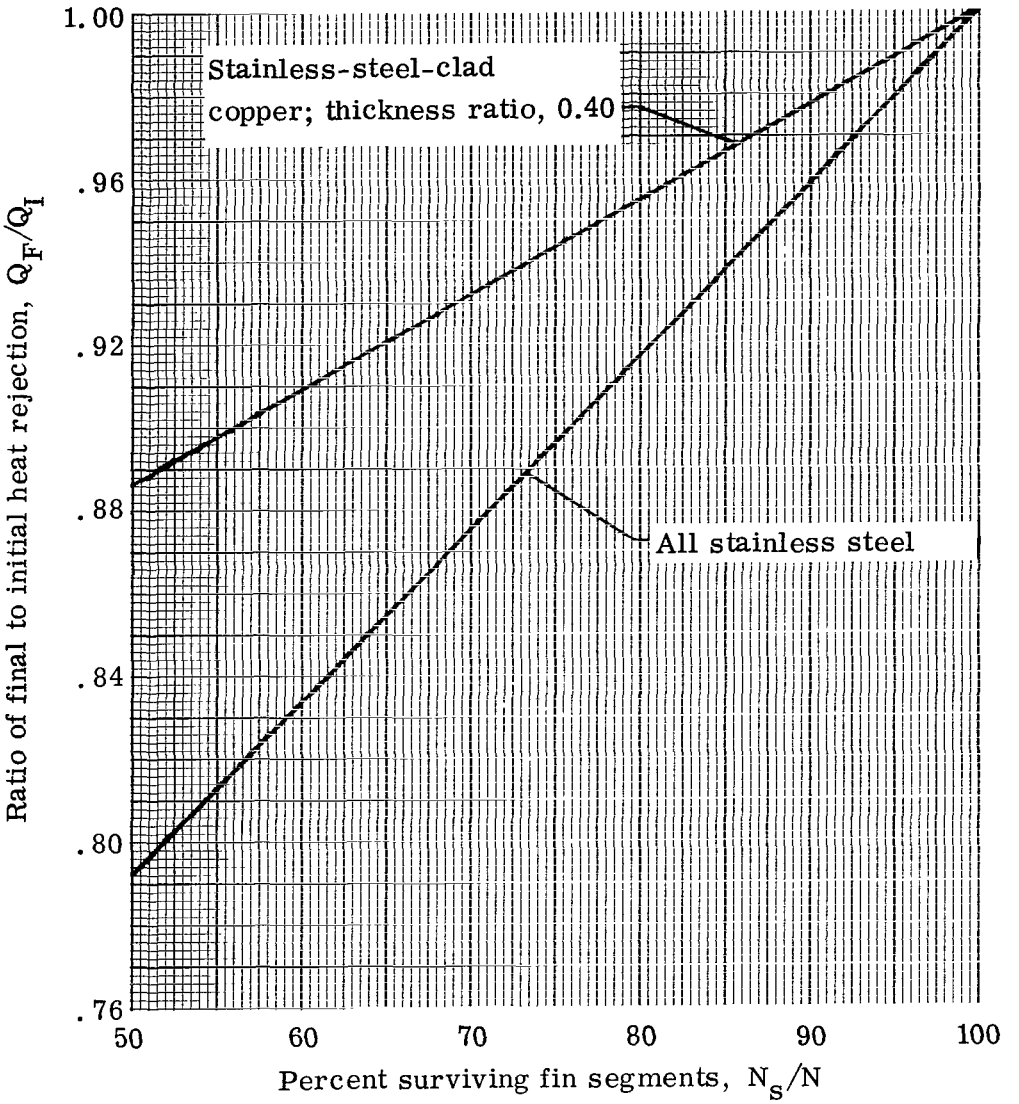

Figure 9. - Effect of number of surviving fin segments on radiator final to initial heat rejection ratio. Vapor-chamber fin-tube radiator; vapor-chamber fin segment planform area, 30 square inches (193.5 cm^2); tube block sidewall thickness ratio, 0.25.

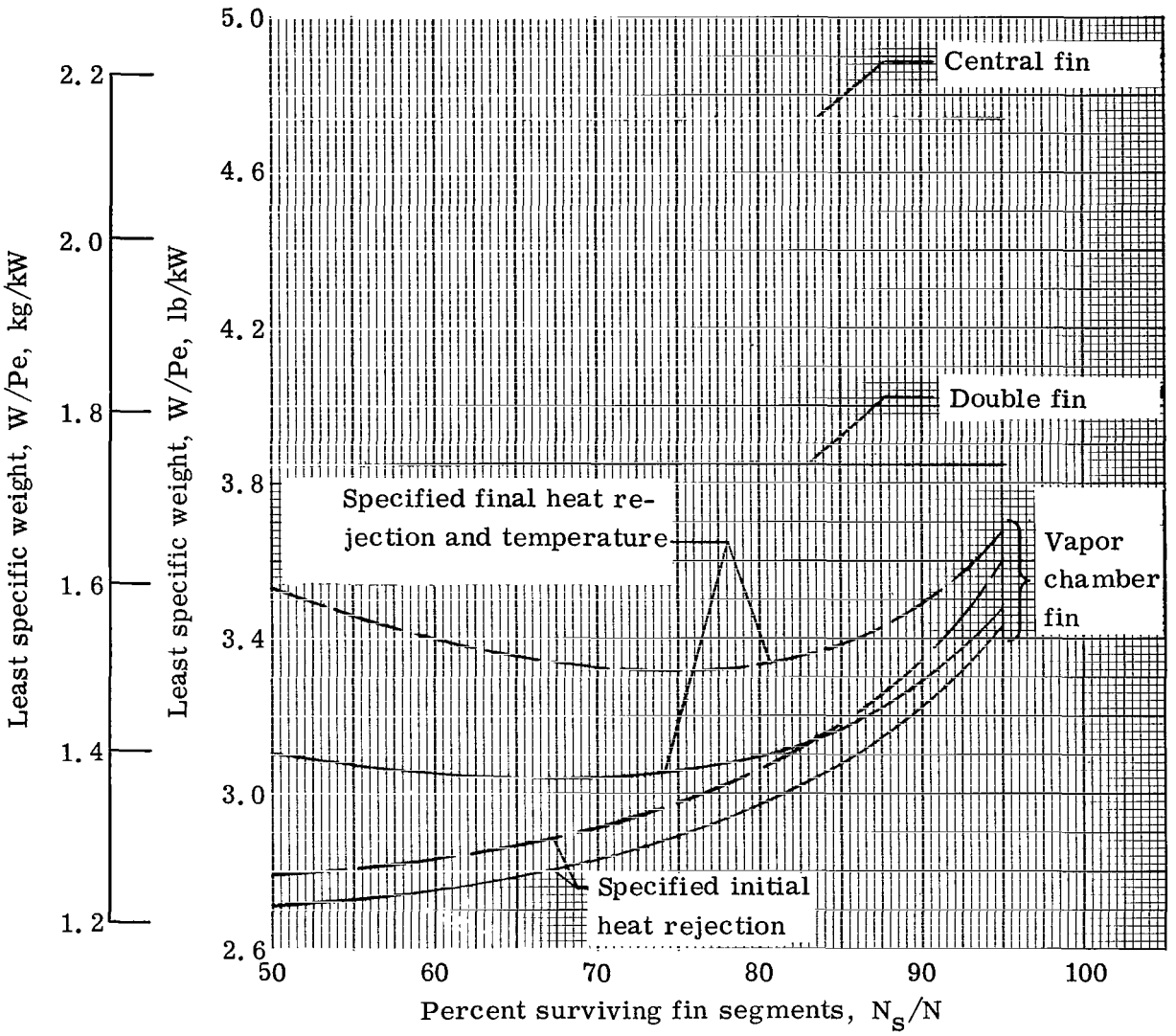

(a) Weight increase based on planform area increase.

Figure 10. - Effect of surviving fin segments on radiator least specific weight. Tube nonpuncture probability, 0.98; tube block sidewall thickness ratio, 0.25; stainless-steel clad to copper thickness ratio, 0.40.

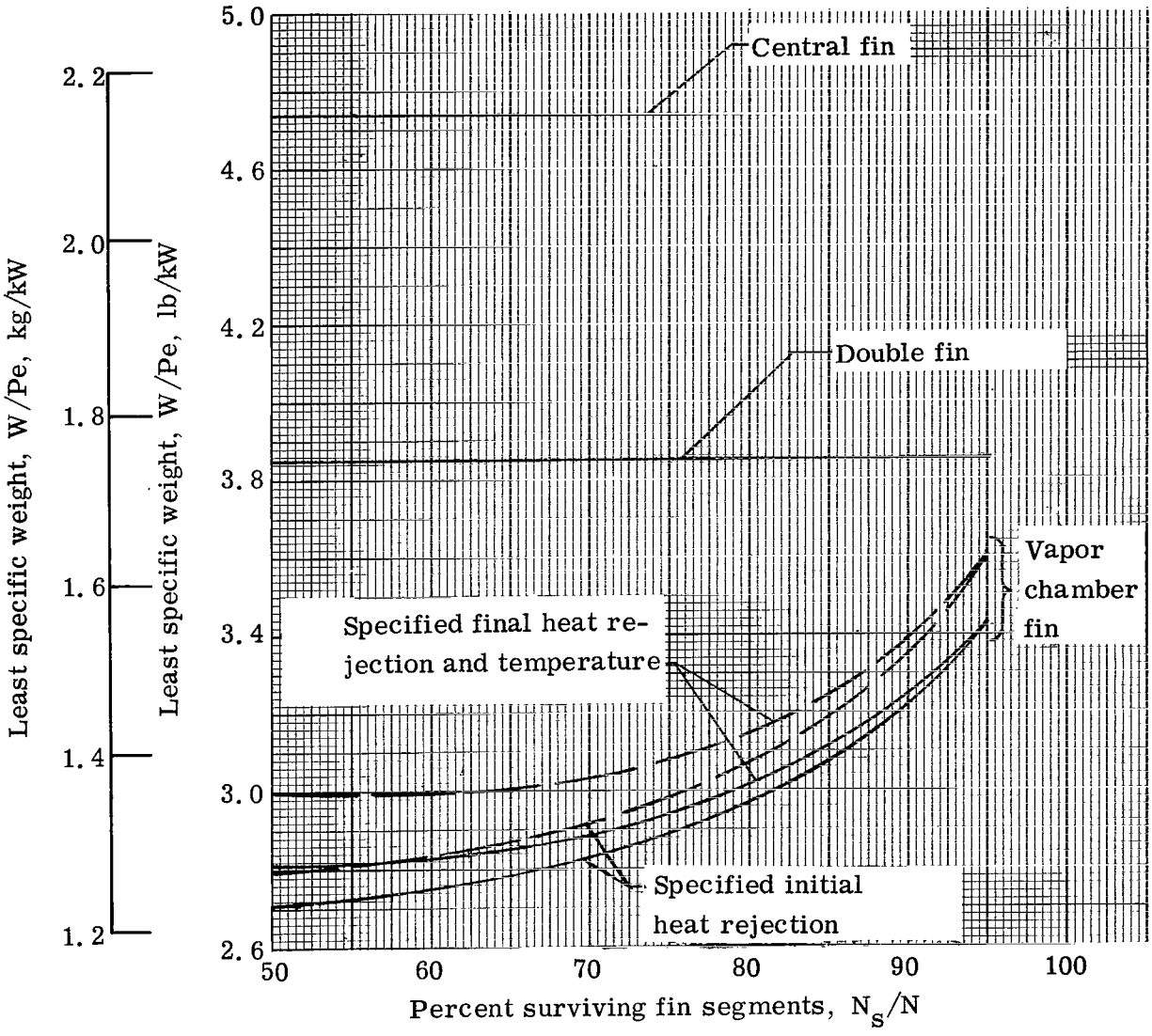

(b) Weight increase based on fin area increase.

Figure 10. - Concluded.

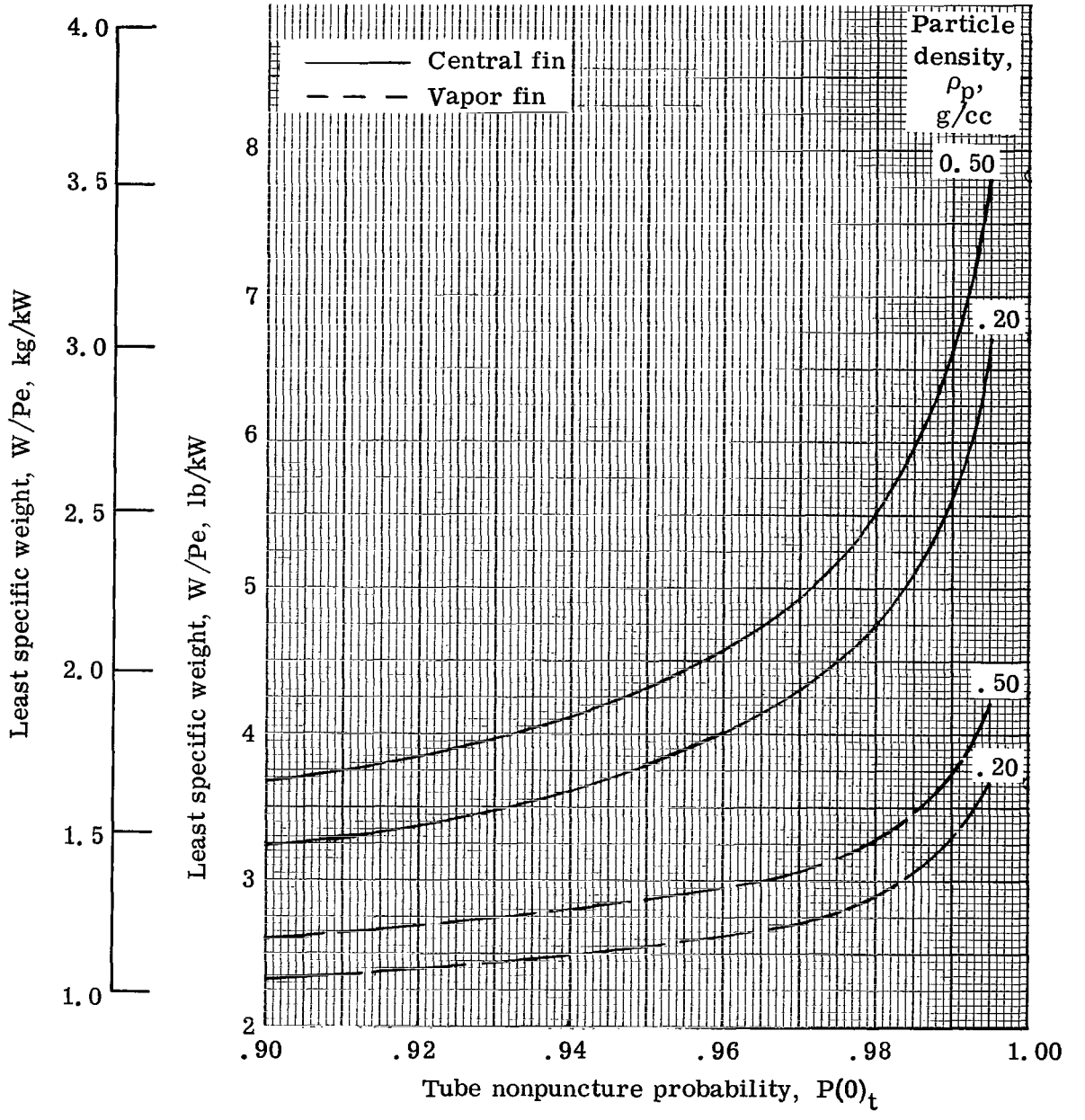

Figure 11. - Effect of meteoroid particle density on radiator least specific weight. Stainless-steel-clad copper fins; percent surviving fin segments, 75; vapor chamber fin segment planform area, 30 square inches (193.5 cm^2); tube block sidewall thickness ratio, 0.25; stainless-steel-clad to copper thickness ratio, 0.40.

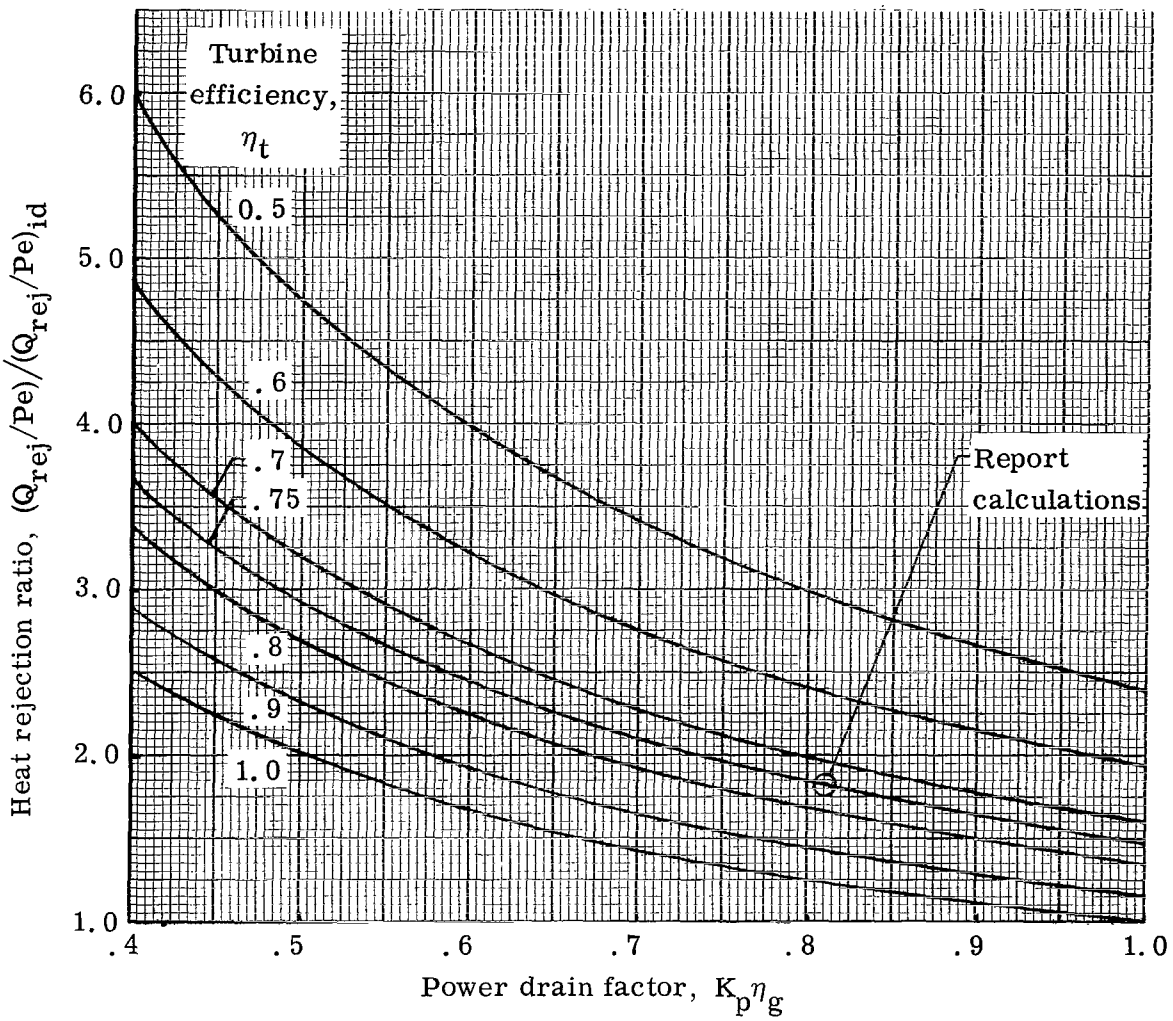

Figure 12. - Variation of heat-rejection ratio with power-drain factor. Turbine inlet to radiator fluid inlet temperature ratio, 0.69; thermodynamic cycle efficiency, 0.281. Ideal case: turbine efficiency, 1.0; generator efficiency, 1.0; power availability factor, 1.0.

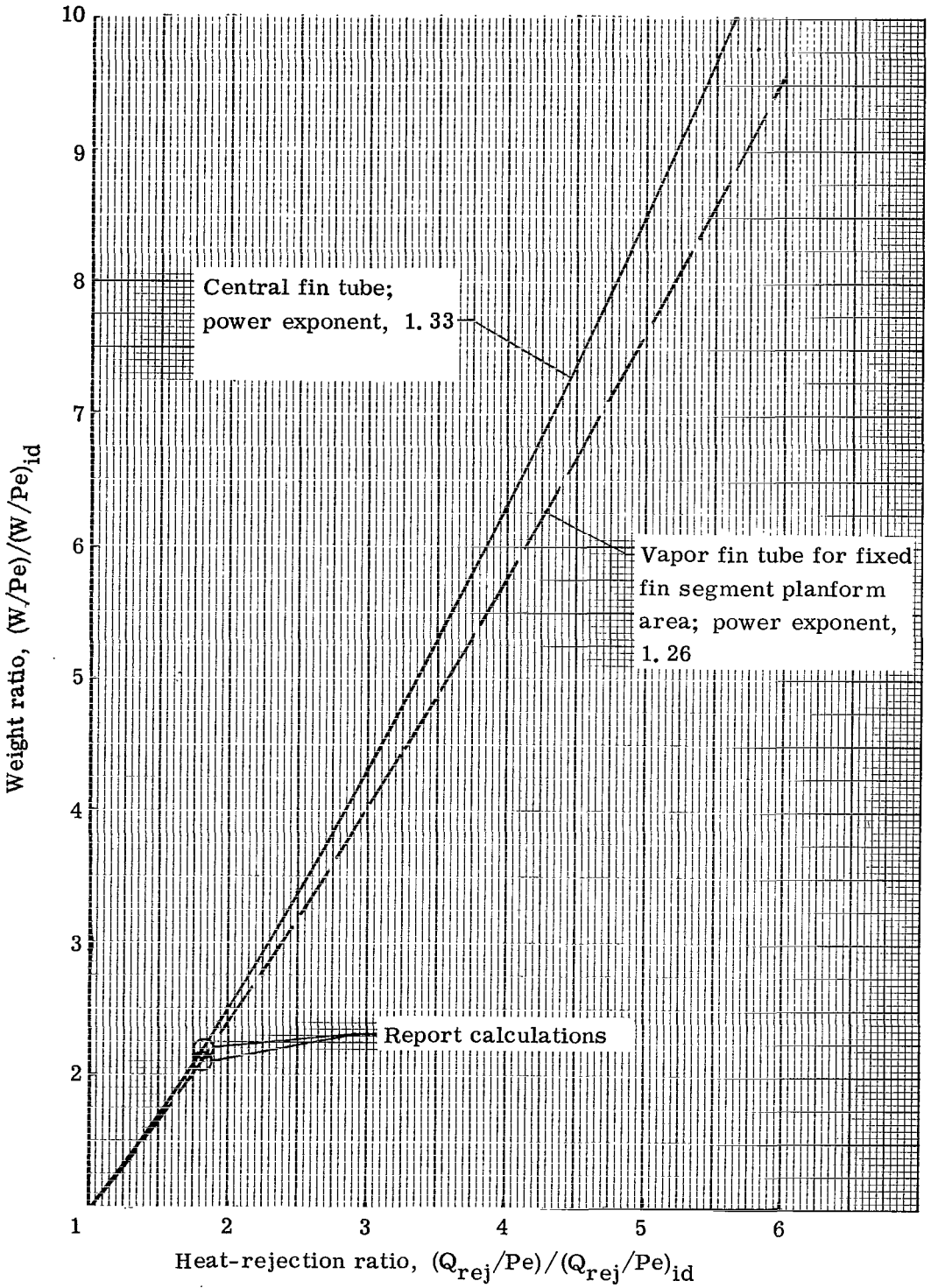

Figure 13. - Variation of radiator weight ratio with heat-rejection ratio. Tube nonpuncture probability, 0.98; stainless-steel clad to copper thickness ratio, 0.40.

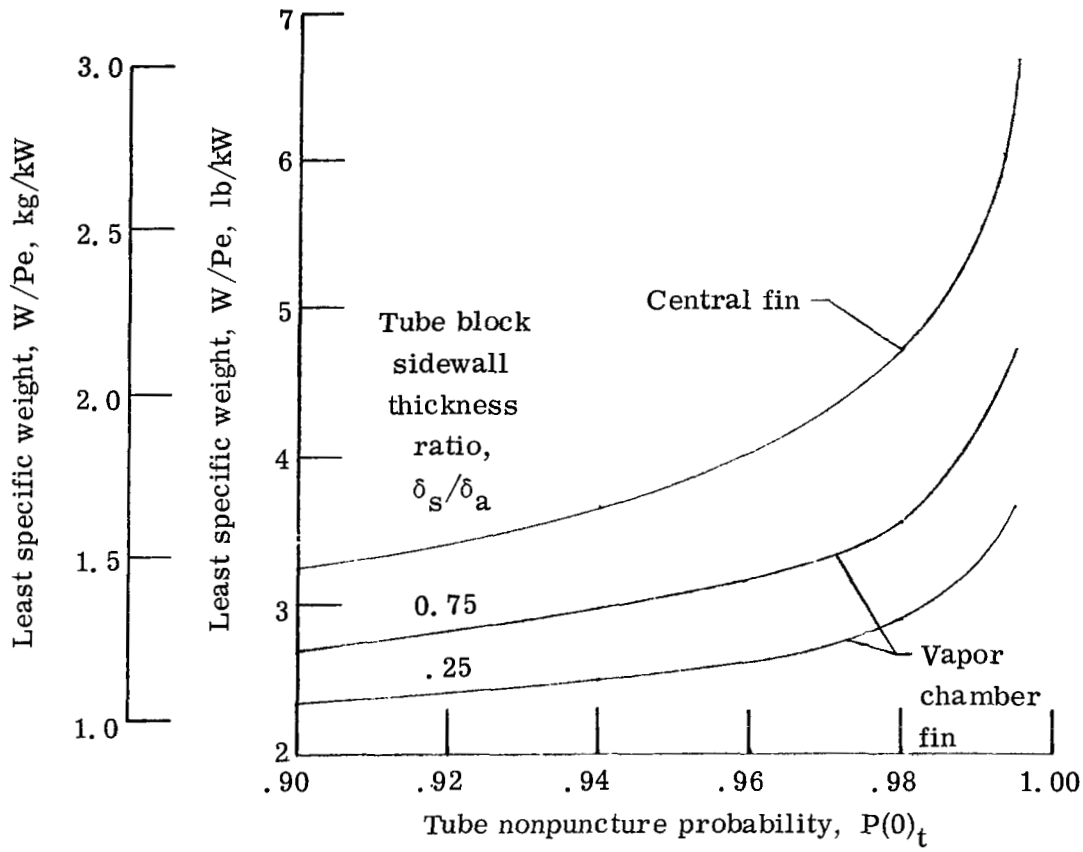

Figure 14. - Effect of tube block sidewall thickness ratio on radiator least specific weight. Stainless-steel clad to copper thickness ratio, 0.40; percent surviving fin segments, 75; vapor-chamber fin segment planform area, 30 square inches (193.5 cm^2).

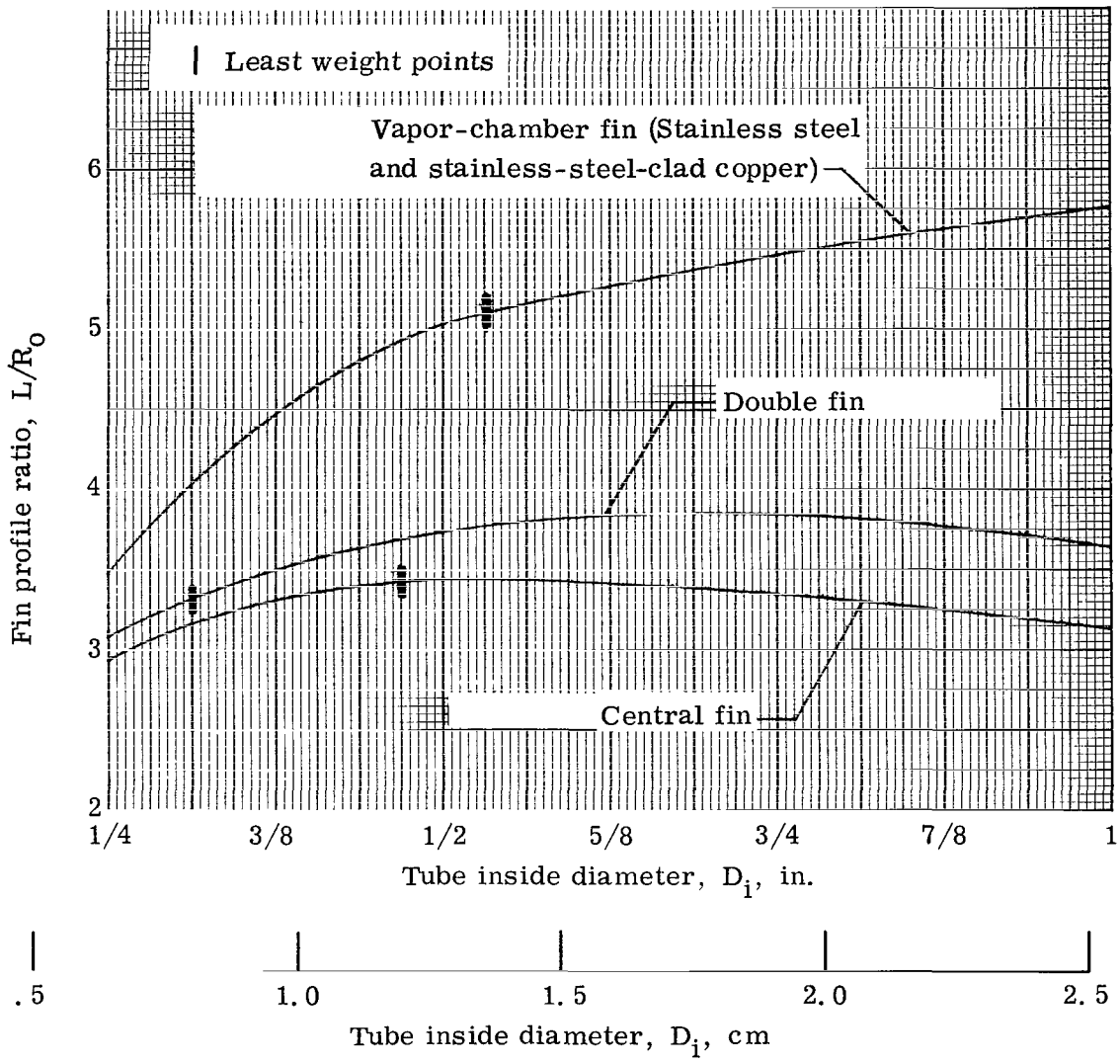

Figure 15. - Variation of fin profile ratio with tube inside diameter at minimum specific weight. Tube nonpuncture probability, 0.98; stainless-steel clad to copper thickness ratio, 0.40; tube block sidewall thickness ratio, 0.25; vapor-chamber fin segment planform area, 30 square inches (193.5 cm^2); percent surviving fin segments, 75.

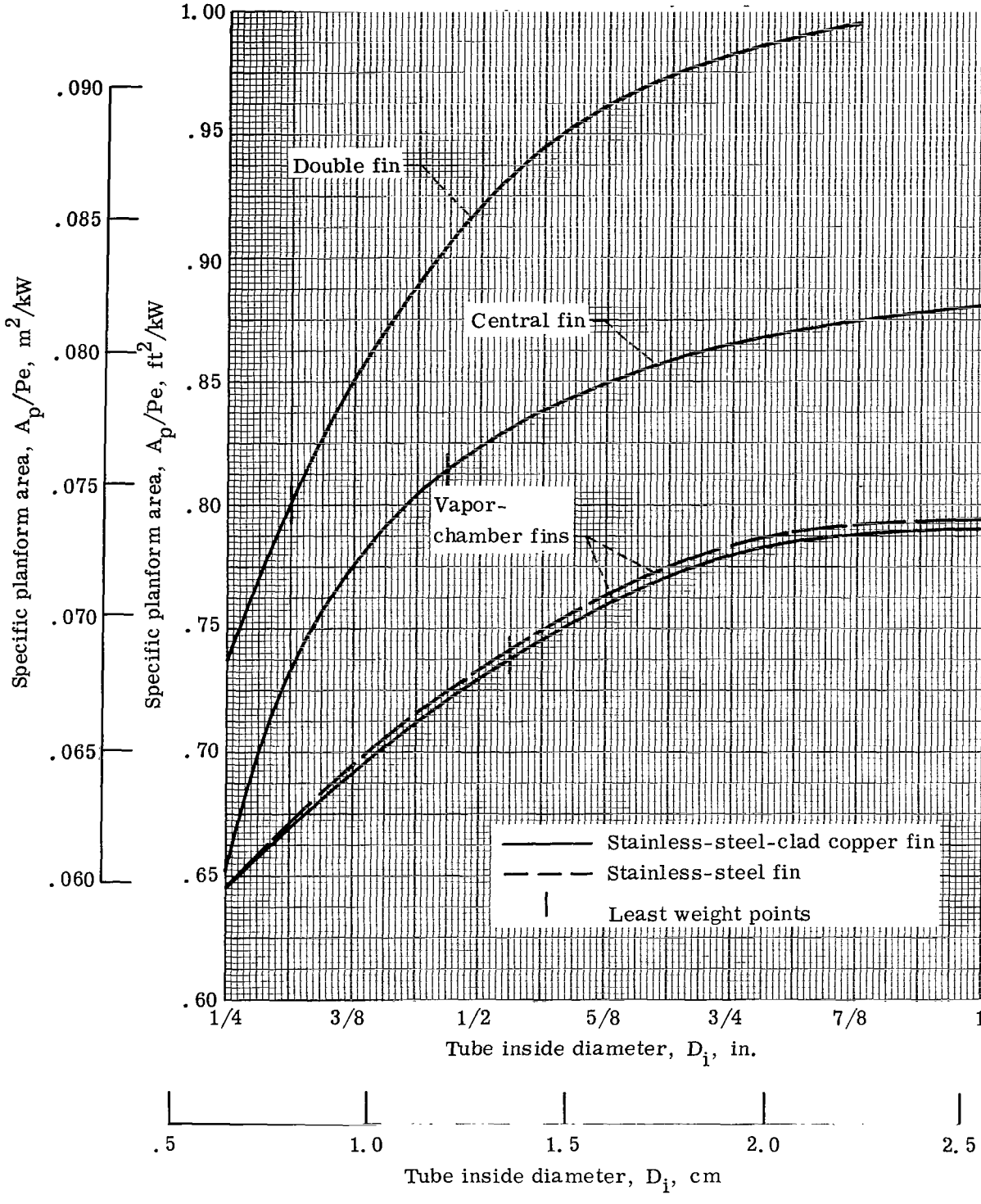

Figure 16. - Variation of radiator specific planform area with tube inside diameter. Tube nonpuncture probability, 0.98; tube block sidewall thickness ratio, 0.25; fin segment planform area, 30 square inches (193.5 cm^2); percent surviving fin segments, 75.

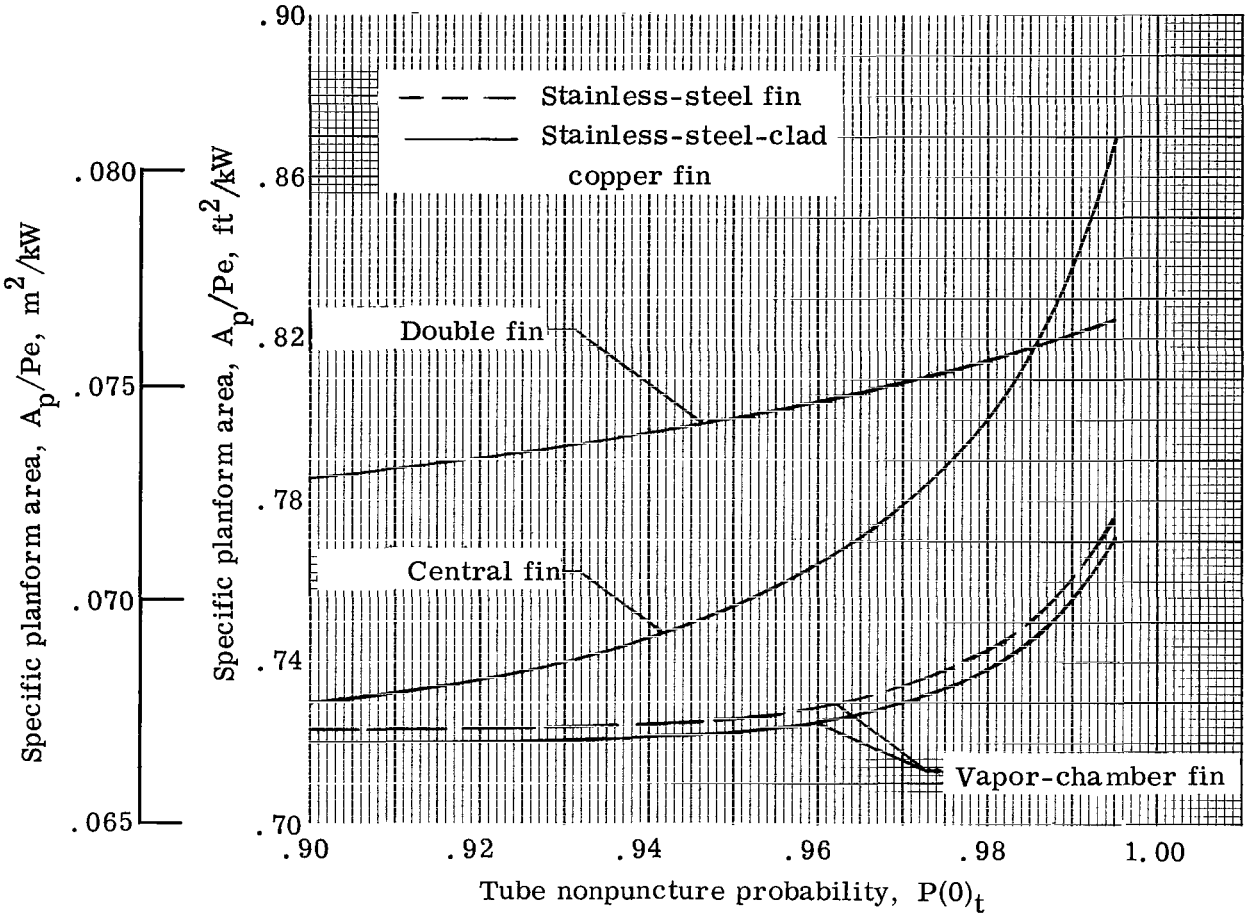

Figure 17. - Variation of radiator specific planform area with tube nonpuncture probability at least-specific-weight. Percent surviving fin segments, 75; fin segment planform area, 30 square inches (193.5 cm^2); tube block sidewall thickness ratio, 0.25.

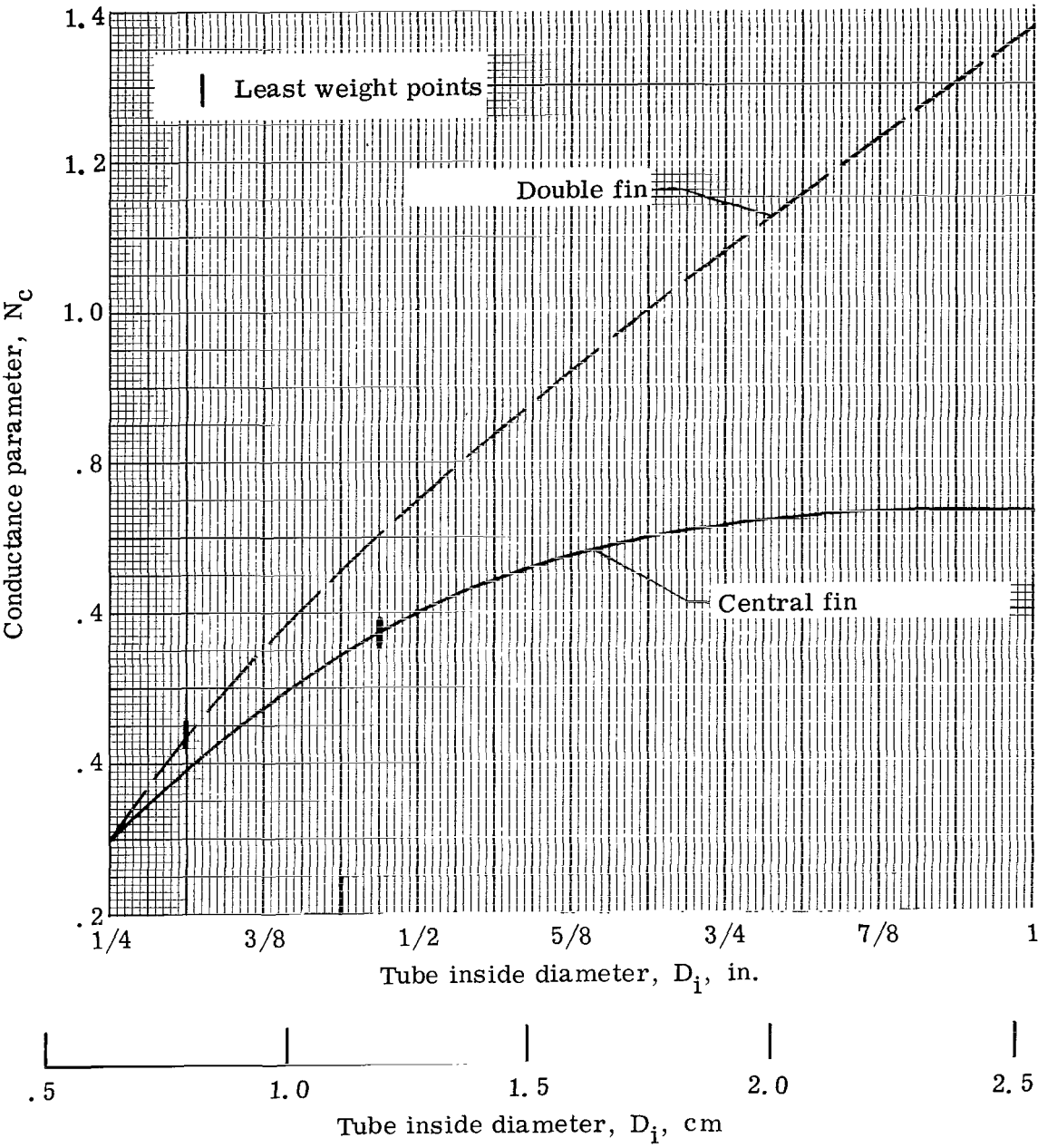

Figure 18. - Conductance parameter at minimum specific weight. Tube nonpuncture probability, 0.98; tube block sidewall thickness ratio, 0.25.

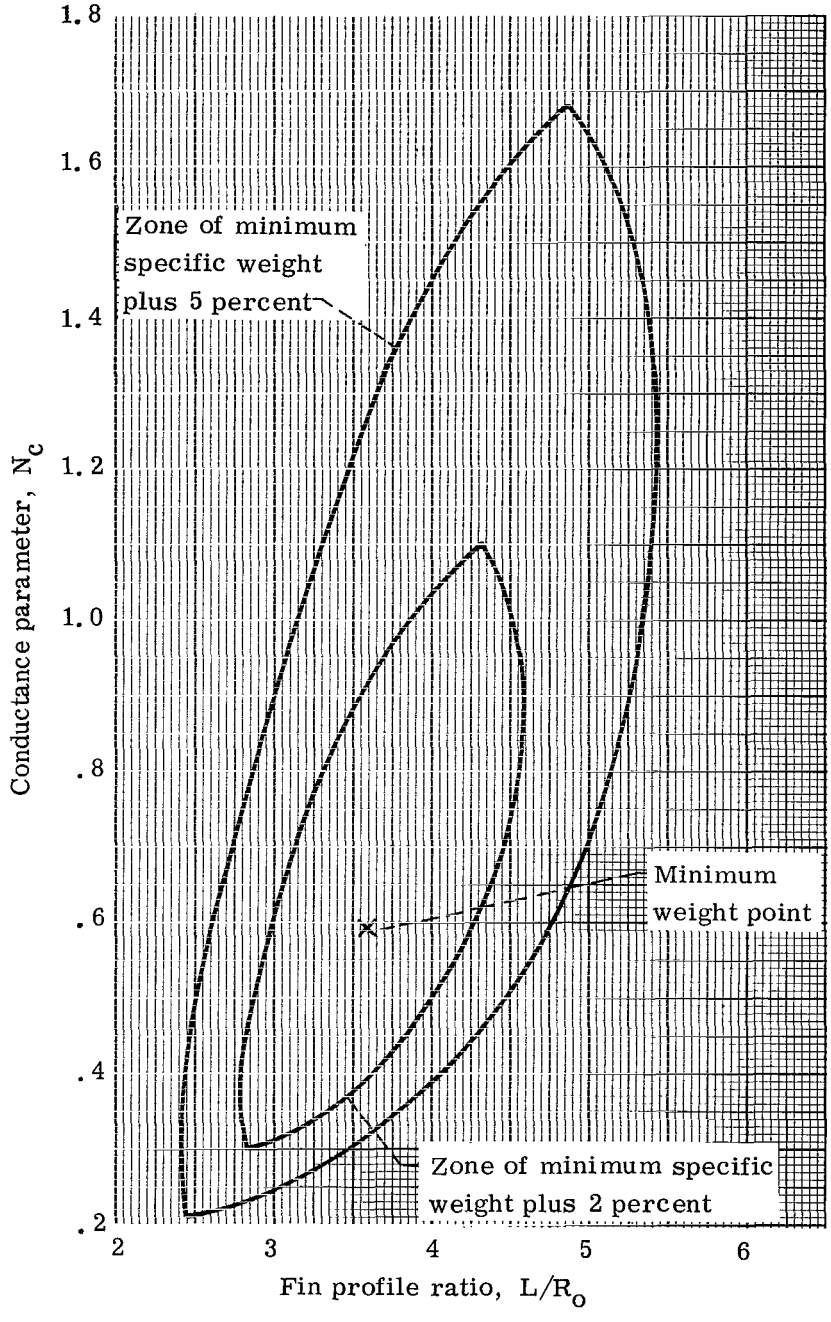

(a) Central fin-tube radiator. Tube inside diameter, 1/2 inch (1.27 cm).

Figure 19. - Zones of solid conducting fin profile ratio and conductance parameter for near minimum weight. Tube nonpuncture probability, 0.98.

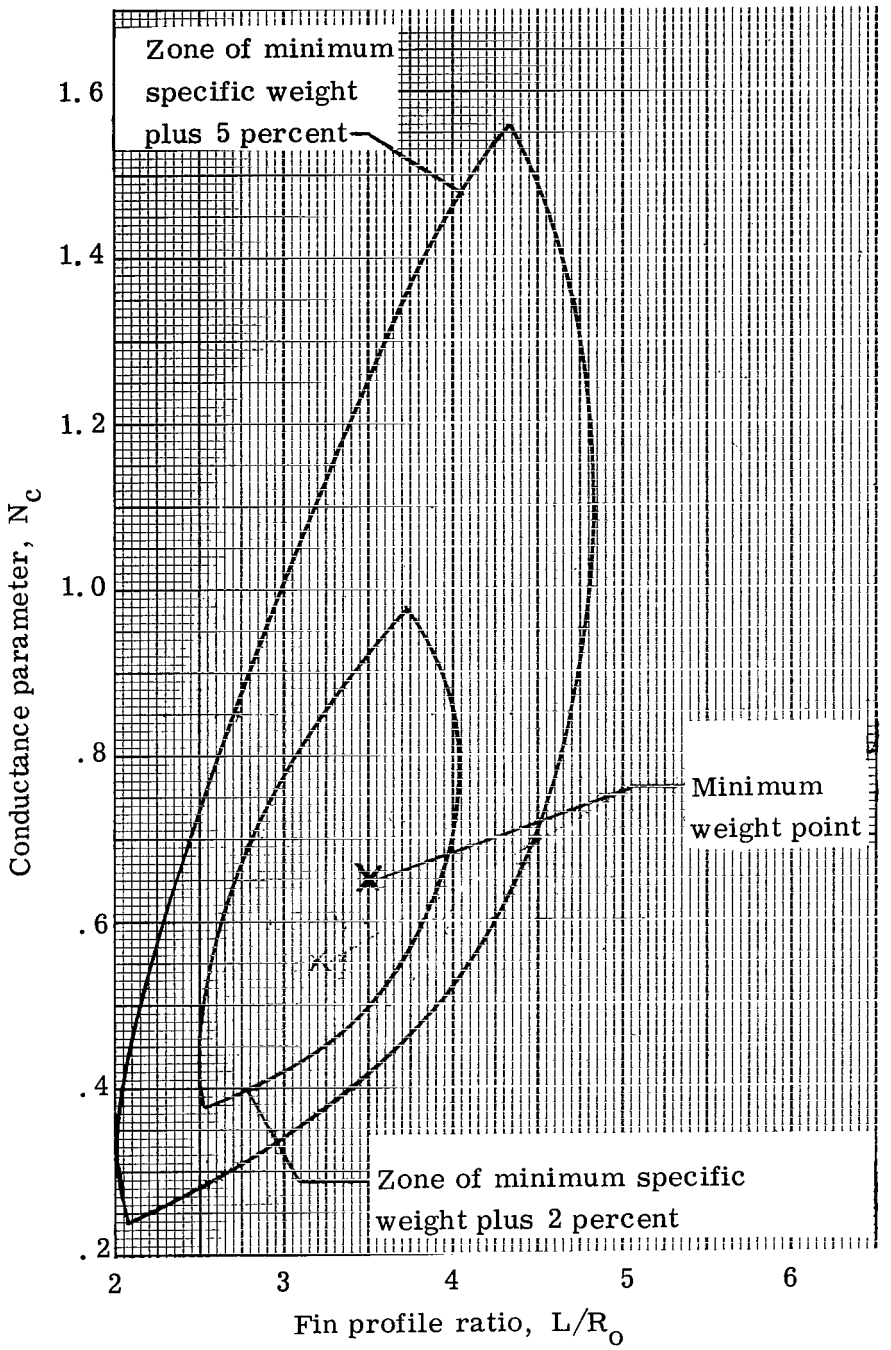

(b) Double fin-tube radiator. Tube block sidewall thickness ratio, 0.25; tube inside diameter, 3/8 inch (0.95 cm).

Figure 19. - Concluded.

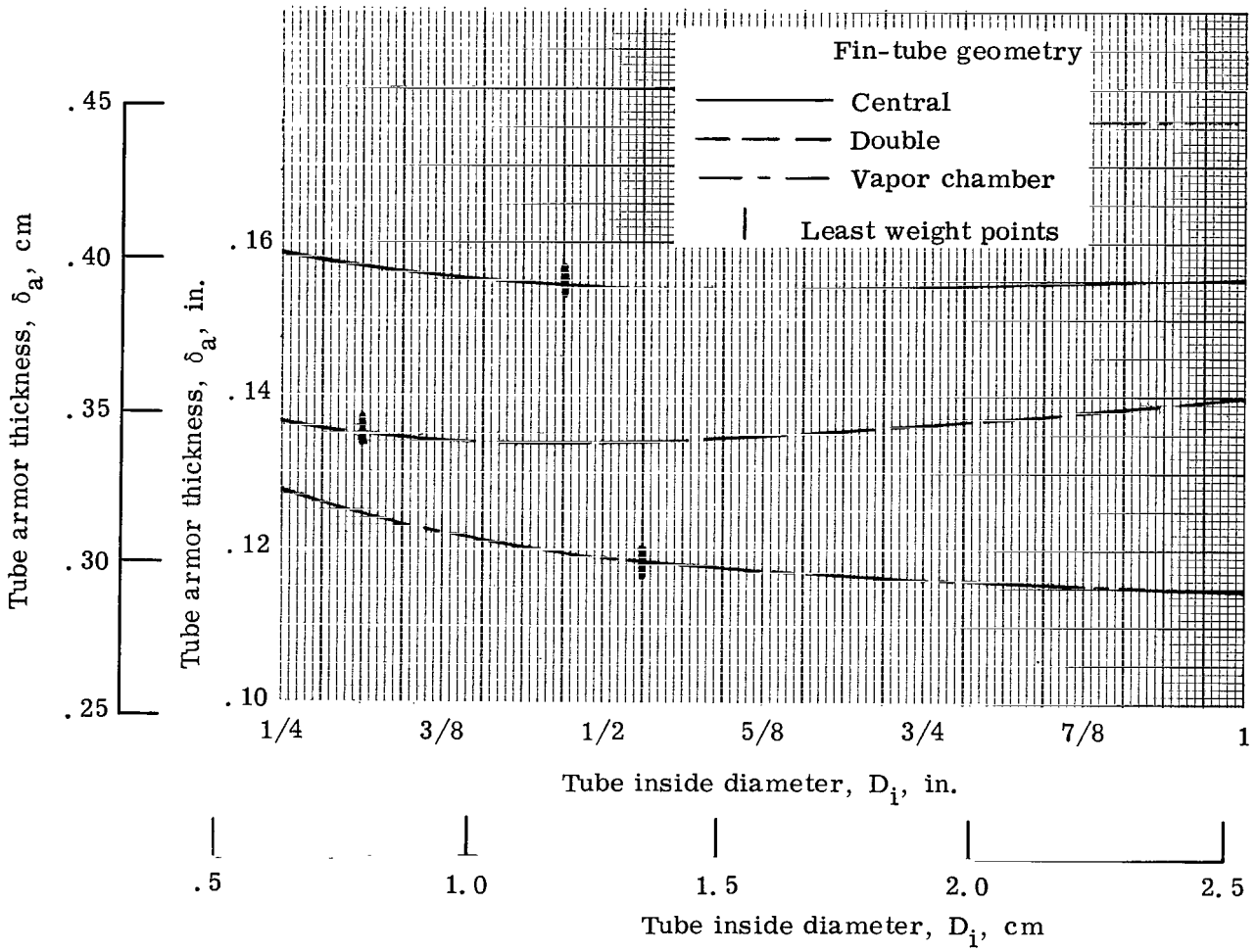

Figure 20. - Variation of tube armor thickness with tube inside diameter at minimum specific weight. Tube nonpuncture probability, 0.98; stainless-steel clad to copper thickness ratio, 0.40; tube block sidewall thickness ratio, 0.25; vapor-chamber fin segment planform area, 30 square inches (193.5 cm^2); percent surviving fin segments, 75.

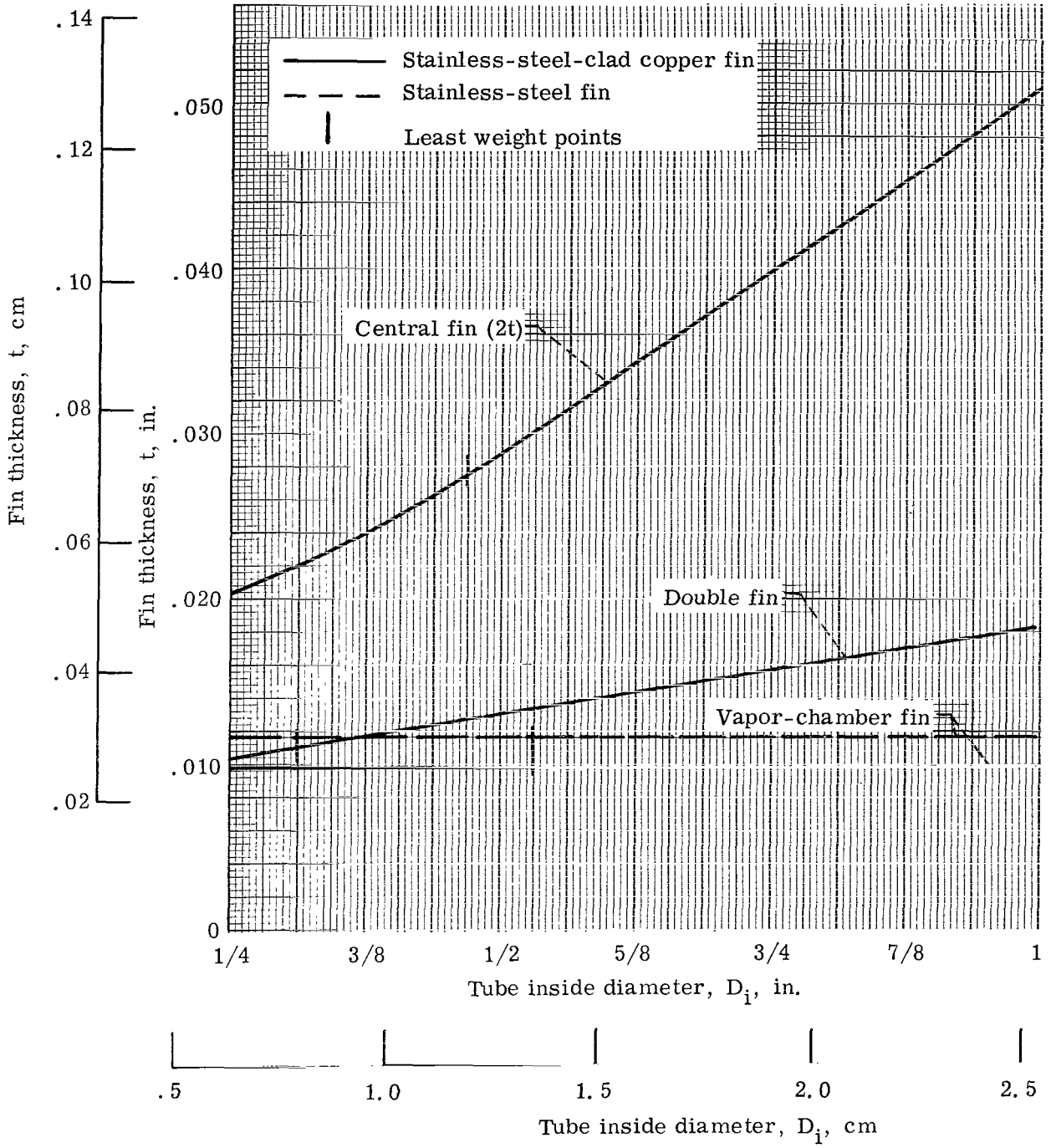

Figure 21. - Variation of fin thickness with tube inside diameter at minimum specific weight. Stainless-steel clad to copper thickness ratio, 0.40; tube nonpuncture probability, 0.98: tube block sidewall thickness ratio, 0.25; percent surviving fin segments, 75; vapor-chamber fin segment planform area, 30 square inches (193.5 cm^2).

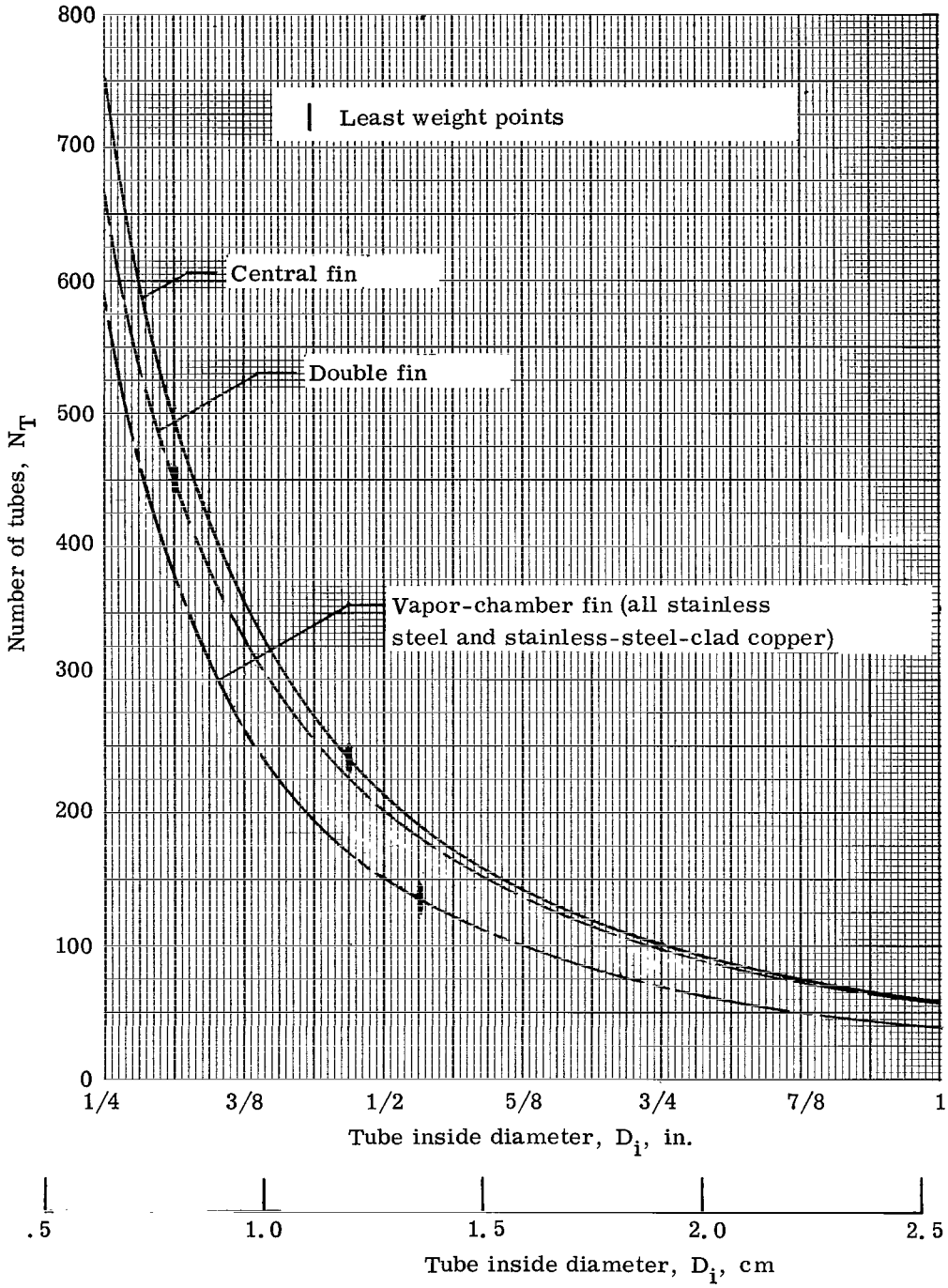

Figure 22. - Variation of number of tubes with tube inside diameter at minimum specific weight. Tube nonpuncture probability, 0.98; stainless-steel clad to copper thickness ratio, 0.40; tube block sidewall thickness ratio, 0.25; vapor-chamber fin segment planform area, 30 square inches (193.5 cm^2); percent surviving fin segments, 75.

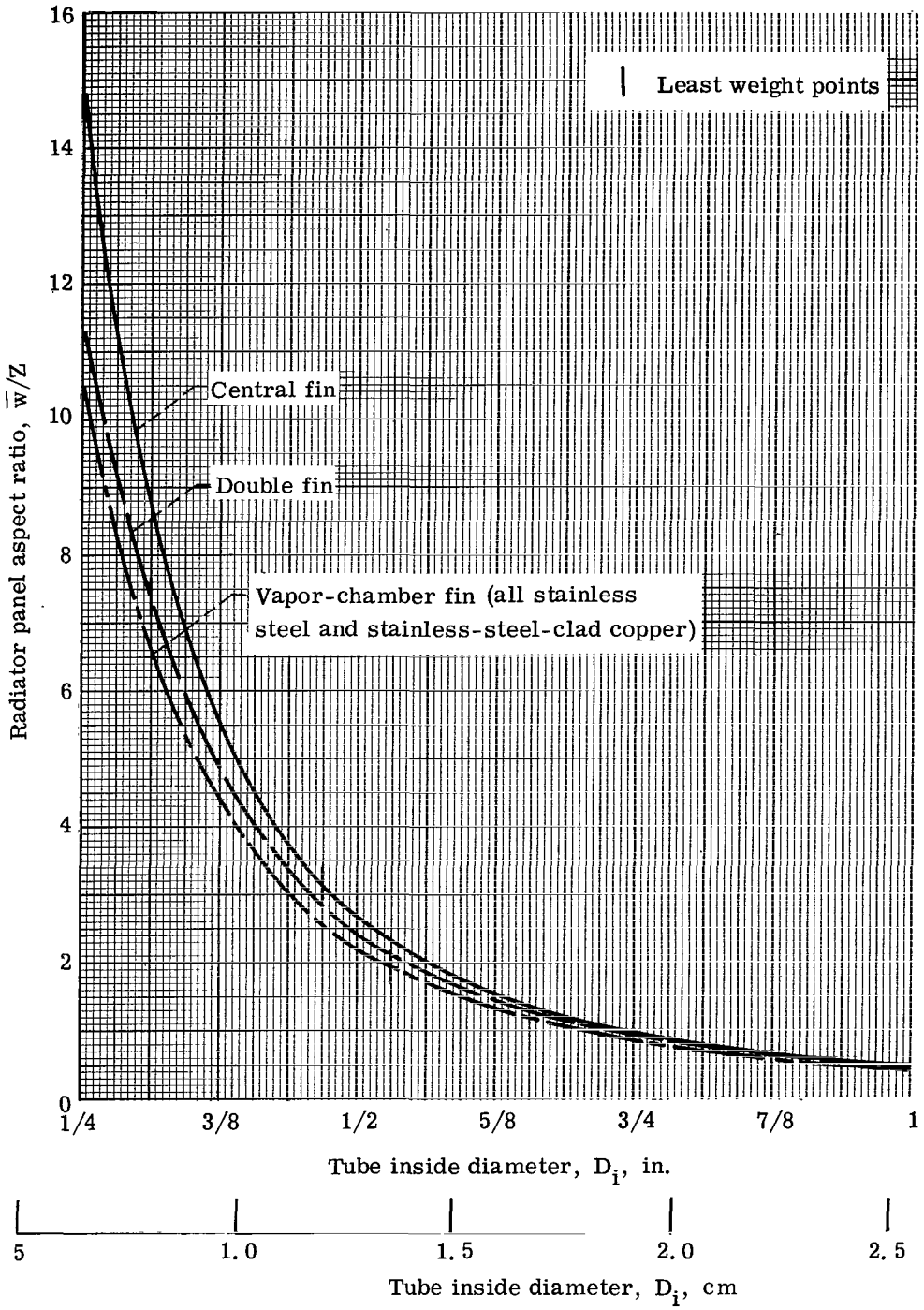

Figure 23. - Variation of panel aspect ratio with tube inside diameter at minimum specific weight. Tube nonpuncture probability, 0.98; stainless-steel clad to copper thickness ratio, 0.40; tube block sidewall thickness ratio, 0.25; vapor-chamber fin segment planform area, 30 square inches (193.5 cm^2); percent surviving fin segments, 75.

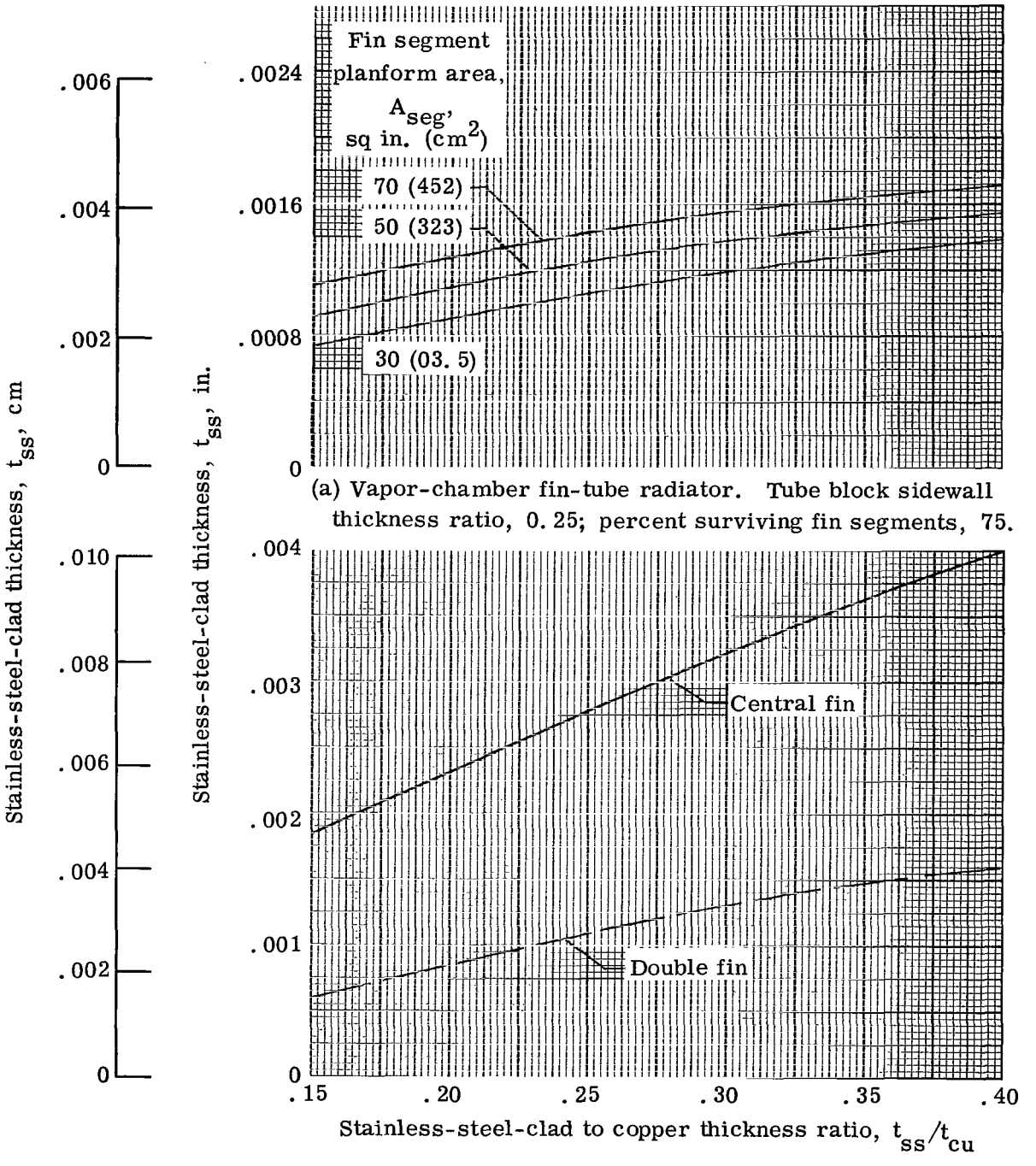

(a) Vapor-chamber fin-tube radiator. Tube block sidewall thickness ratio, 0.25; percent surviving fin segments, 75.

(b) Central and double fin-tube radiators. Double fin tube block sidewall thickness ratio, 0.25.

Figure 24. - Variation of stainless-steel clad thickness with material thickness at least radiator specific weight. Tube nonpuncture probability, 0.98.

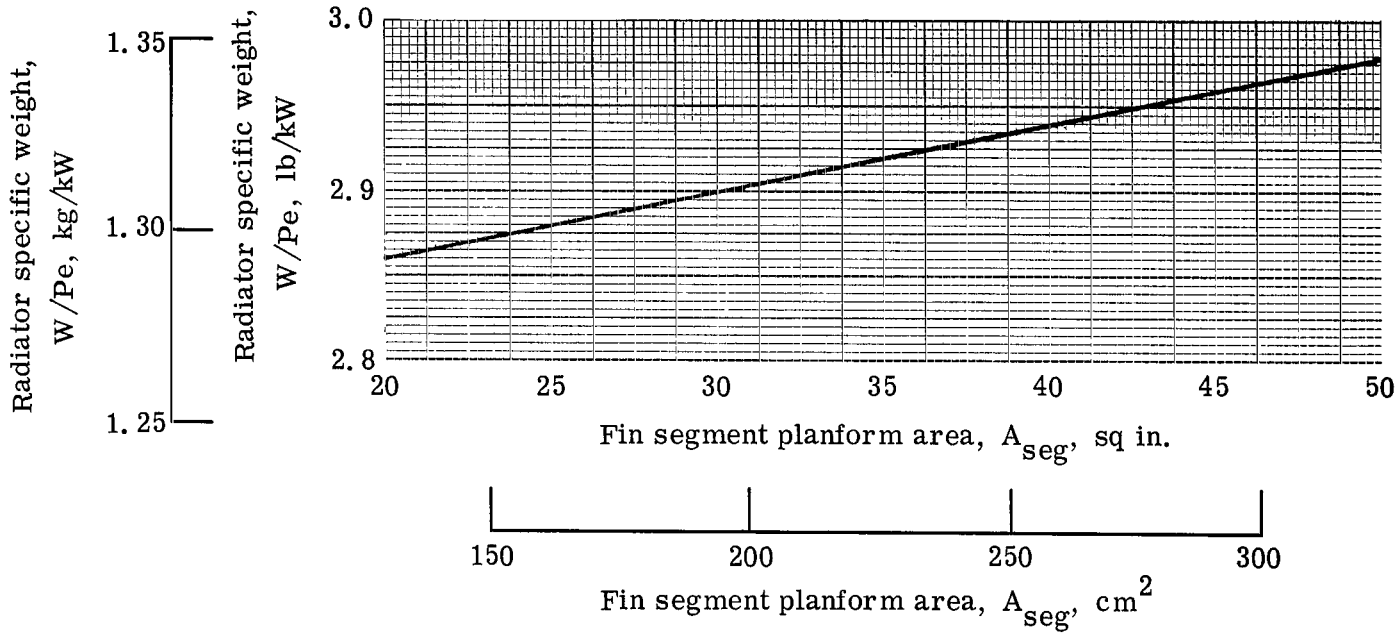

Figure 25. - Variation of least specific weight with fin segment planform area. Stainless-steel clad to copper thickness ratio, 0.40; tube nonpuncture probability, 0.98; percent surviving fin segments, 75; tube block sidewall thickness ratio, 0.25.

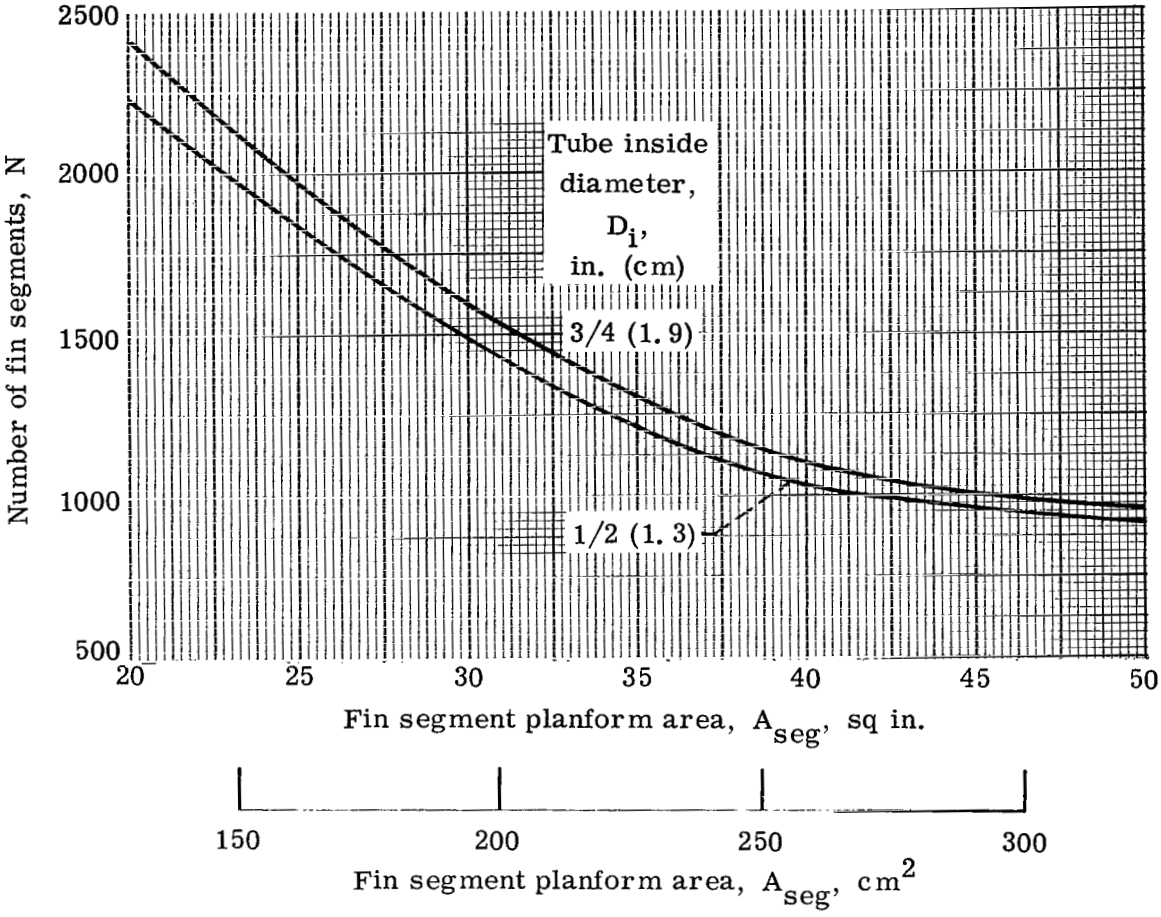

Figure 26. - Variation of number of fin segments with fin segment planform area at least specific weight. Tube nonpuncture probability, 0.98; percent surviving fin segments, 75; tube block sidewall thickness ratio, 0.25.

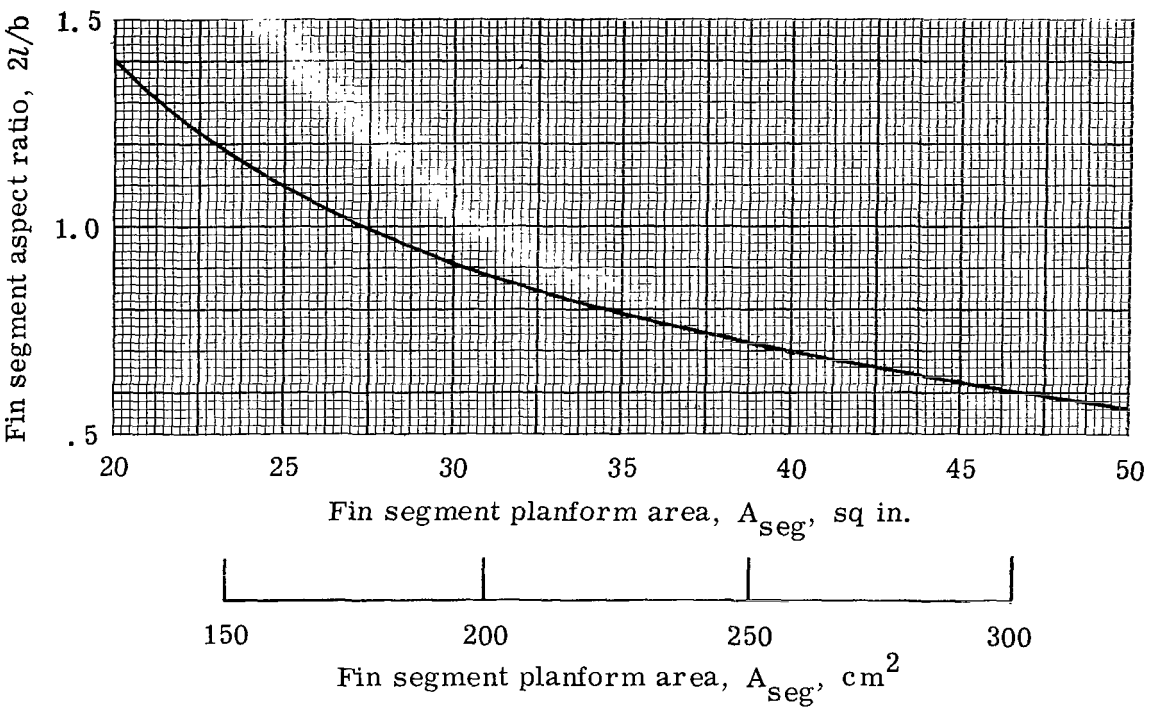

Figure 27. - Variation of fin segment aspect ratio with fin segment planform area at least specific weight. Tube nonpuncture probability, 0.98; percent surviving fin segments, 75; tube inside diameter, 3/4 inch (1.904 cm); tube block sidewall thickness ratio, 0.25.

NASA-Langley, 1968 —— 33 E-3972

"The aeronautical and space activities of the United States shall be conducted so as to contribute . . . to the expansion of human knowledge of phenomena in the atmosphere and space. The Administration shall provide for the widest practicable and appropriate dissemination of information concerning its activities and the results thereof."

—NATIONAL AERONAUTICS AND SPACE ACT OF 1958

NASA SCIENTIFIC AND TECHNICAL PUBLICATIONS

TECHNICAL REPORTS: Scientific and technical information considered important, complete, and a lasting contribution to existing knowledge.

TECHNICAL NOTES: Information less broad in scope but nevertheless of importance as a contribution to existing knowledge.

TECHNICAL MEMORANDUMS: Information receiving limited distribution because of preliminary data, security classification, or other reasons.

CONTRACTOR REPORTS: Scientific and technical information generated under a NASA contract or grant and considered an important contribution to existing knowledge.

TECHNICAL TRANSLATIONS: Information published in a foreign language considered to merit NASA distribution in English.

SPECIAL PUBLICATIONS: Information derived from or of value to NASA activities. Publications include conference proceedings, monographs, data compilations, handbooks, sourcebooks, and special bibliographies.

TECHNOLOGY UTILIZATION PUBLICATIONS: Information on technology used by NASA that may be of particular interest in commercial and other non-aerospace applications. Publications include Tech Briefs, Technology Utilization Reports and Notes, and Technology Surveys.

Details on the availability of these publications may be obtained from:

SCIENTIFIC AND TECHNICAL INFORMATION DIVISION

NATIONAL AERONAUTICS AND SPACE ADMINISTRATION

Washington, D.C. 20546